



## Leak Detection in Urban Hydraulic Systems Using the K-BiLSTM-Monte Carlo Dropout Model

Edgar Orlando Ladino-Moreno <sup>1\*</sup>, César Augusto García-Ubaque <sup>1</sup>

<sup>1</sup> Department of Civil Engineering, Universidad Distrital Francisco José de Caldas, Bogotá, Colombia.

Received 02 April 2024; Revised 18 June 2024; Accepted 24 June 2024; Published 01 July 2024

### Abstract

Utility companies lose approximately 35 liters of water for every 100 produced due to incorrect, illegal connections and the poor condition of pipes. This study develops an intelligent model to detect leaks using the Kalman filter, BiLSTM neural networks, and the Monte Carlo Dropout algorithm. Using data from the Empresa de Acueductos y Alcantarillados de Bogotá (EAAB), Colombia, autocorrelation analysis, PCA, cluster analysis, ADF and Durbin-Watson tests, Hurst exponent, spectral analysis, and wavelet transform were performed. Then, Kalman filtering techniques were applied, and a BiLSTM architecture controlled with Monte Carlo dropout was implemented. The results showed an accuracy of 87.48% in training and 80.48% in validation. Temporal analysis revealed a stationary behavior in the flow series, and the decrease in spectral intensity around 0.25 Hz was related to pressure perturbations caused by leaks. A detailed evaluation of pressure and flow signals identified leak patterns with high precision, demonstrating the effectiveness of the wavelet spectrogram in detecting energy disturbances. The novelty of the study lies in the integration of advanced artificial intelligence and combinatorial optimization techniques to improve water resource management, allowing early and accurate detection of leaks, significantly improving compared to traditional methods.

*Keywords:* BiLSTM; Kalman Filtering; Leak; Monte Carlo Dropout; Public Utility Management; Spectral Analysis; Wavelet Transform.

## 1. Introduction

The sustainability of water resources in urban centers is currently compromised by the loss of water in distribution systems, due to both commercial and technical losses. These leaks cause secondary effects on urban infrastructure, such as soil erosion, deterioration of roads, and increased operating costs. The high demand for water in large cities forces service providers to implement mechanisms and plans to manage this problem. Therefore, the adoption of disruptive technologies in hydraulic systems is essential, allowing the development of intelligent and resilient systems. Consequently, the current development of combinatorial models for leak detection and quantification requires the adoption of deep learning algorithms that identify patterns in time series. Traditional deterministic methods are not sufficient to approximate effective solutions, underscoring the need to combine real-time monitoring techniques with artificial intelligence and expert knowledge. The study of signals in the field of hydraulics, both under pressure and free flow, is essential to capture the dynamics of the system, given the inherent complexity due to the multiplicity of variables and parameters involved in hydraulic systems. The integration of artificial intelligence (AI), the Internet of Things (IoT), and expert knowledge enables the creation of intelligent hydraulic systems. These systems not only learn from demand patterns but are also resilient and autonomous, managing critical eventualities instantly.

This combination optimizes the efficiency and responsiveness of hydraulic systems to various operating conditions (WDNs). Thus, Yang & Zhao (2021) [1] present an advanced method for detecting and locating leaks in pipelines using

\* Corresponding author: [eoladinom@udistrital.edu.co](mailto:eoladinom@udistrital.edu.co)

 <http://dx.doi.org/10.28991/CEJ-2024-010-07-01>



© 2024 by the authors. Licensee C.E.J, Tehran, Iran. This article is an open access article distributed under the terms and conditions of the Creative Commons Attribution (CC-BY) license (<http://creativecommons.org/licenses/by/4.0/>).

deep learning techniques. This method effectively distinguishes between disturbances and real leaks, thus minimizing the incidence of false alarms and localization errors in both experimental tests and simulations. In the study by Zhang et al. (2023) [2], an attention mechanism (AM) combined with LSTM networks is used to optimize the detection and localization of natural gas leaks. The AM is used to assign relevant initial weights, while the LSTM is responsible for identifying correlations in the data. This approach was validated in an urban gas network, obtaining high precision with an AUC of 0.99. The proposed methodology significantly improves the reliability of the system, highlighting the sensors close to the leaks for more accurate detection. For this reason, it is essential to implement hydraulic systems in real-time to detect transient events caused by disturbances in the system, such as leaks. For example, Yang & Zhao (2020) [3], propose a continuous pressure monitoring system and pressure point analysis (PPA) for the detection of leaks in pipelines. However, this model has high false alarm rates. To improve accuracy and reduce false alarms, a model based on OPELM and BiLSTM is used. Experiments conducted with real data have demonstrated the effectiveness of this approach, improving the practicality of pressure monitoring for leak detection.

According to Wang et al. (2024) [4], it is essential to establish monitoring of the characteristics of pipes to prevent leaks and damage. Therefore, it proposes an advanced technique based on GTFE-Net, BiLSTM, and an attention mechanism (GTFE-Net-BiLSTM-AM) to improve the accuracy of 93.7% in deformation recognition. Therefore, it is possible to establish monitoring of acoustic emissions in industrial pipes to detect leaks. Gao et al. (2022) [5] suggested a hybrid approach that uses minimum entropy deconvolution together with frequency energy buffering to optimize the identification of relevant signals and eliminate noise in time series. This method analyzes the changes in the envelope and the temporal difference of the acoustic waves, allowing precise location of leaks. This technique outperforms traditional cross-correlation and empirical modal decomposition methods in terms of accuracy. Guo et al. (2012) [6], a frequency domain inverse method is suggested for pipeline leak detection, which analyzes the differences in the transient response of hydraulic loading between simulated and measured data.

Ullah et al. (2023) [7] recommend a leak detection platform that employs machine learning and acoustic emission (AE) technology. This approach extracts features from AE signals to train models, including neural networks and random forests. By evaluating four data sets, the system achieved 99% accuracy in detecting leaks of various sizes. Shen & Cheng (2022) [8] stated that machine learning techniques can significantly improve leak detection in water distribution systems (WDS). Acharya et al. (2023) [9] described an artificial neural network (ANN) model designed to locate leaks in water distribution systems. This model incorporates the use of a robot equipped with an acoustic sensor to capture leak signals, which are subsequently processed using the Discrete Wavelet Transform (DWT). The model was evaluated on a robot test bench and a simulated system, demonstrating 100% accuracy in detecting and locating leaks. Hydraulically, leaks are associated with variations in system pressure and flow, so real-time monitoring of the distribution network is essential to identify these anomalies. The demands generated by users must establish a timeline that allows recognition of consumption patterns and determining the spectral footprint of demand by hydraulic sectors. This requires characterizing each sector in terms of spectral frequencies so that disturbances in the spectrum can be detected when behavior changes due to leakage. Using advanced signal analysis and machine learning techniques, leaks can be detected and located more accurately and quickly, improving the efficiency and reliability of the water distribution system. Lee & Kim (2023) [10] analyzed the essential characteristics of data collected by leak detection sensors in meter boxes and water pipe outlets. The data is preprocessed and applied to machine learning models. XGBoost is selected as the most suitable model with an accuracy of 99.79%, effectively reducing leak detection and response, minimizing water waste and economic losses in various fields with water pipelines.

In this context, Chumchu (2021) [11] developed a home-based water leak detection system using a bidirectional LSTM (BiLSTM) machine learning model. This model is based on historical and experimental water consumption data and is compared with closed recurrent units (GRU) and autoregressive models, evaluating metrics such as the mean square error (MSE), the root mean square error (RMSE), the mean absolute percentage error (MAPE), and the mean absolute error (MAE). The results indicate that the BiLSTM model exhibits superior performance in water leak detection compared to other evaluated approaches. Barandouzi et al. (2012) [12] implemented a Bayesian approach using the Markov chain Monte Carlo method to map leaks. This approach uses physical parameters and quality, pressure, and flow measurements, and the analysis is performed using @Epanet software. The probability function is developed from routine measurements of water quality, pressure, and flow, along with uncertainty in demand. On the other hand, Proença et al. (2023) [13] proposed a simplified analytical model to analyze the soil surface and locate leaks with minimal interference. The study uses seismic compression and Rayleigh wave trajectories to calculate travel time curves. Monte Carlo simulations were performed to improve precision, obtaining a maximum absolute error of 15 cm. In addition, a parametric study improved precision by 27.4%. Zhang et al. (2022) [14] developed a model based on support vector machines (SVM) optimized using a simulated annealing algorithm (SAA-SVM).

This algorithm optimizes the parameters of the SVM, improving its precision and avoiding local optimal solutions. In the laboratory, leak data is collected under various conditions and entered into the SAA-SVM model for optimization using machine learning. The results show that the optimized model quickly and accurately predicts leak shape and loss. The deterministic approach to locating and quantifying leaks in drinking water distribution systems has not provided an effective solution.

Wang et al. (2024) [4] proposed a technique based on GTFE-Net, BiLSTM, and an attention mechanism (AM), called GTFE-Net-BiLSTM-AM. GTFE-Net enhances the time-frequency warping signal, which is fed into the BiLSTM model to extract spatio-temporal features. The results show an accuracy of 93.7%, surpassing existing models by more than 0.9%. The proposed technique improves the safety and operation of gas pipelines. The reduction of variables and dimensionality has led to the development of linear models that do not adequately represent the dynamics of leaks in systems. Therefore, it is important to adopt a change of approach, considering the perspective of complex systems, to address the problem of leaks in pressurized hydraulic systems. Yang & Zhao (2020) [3], a method is proposed that uses the optimized extreme learning machine (OPELM) for preliminary leak detection and the bidirectional long- and short-term memory (BiLSTM) network to identify true positives, reducing false alarms. Furthermore, a feature extraction mechanism is introduced to obtain dynamics and statics of the pressure wave. Experiments on global data sets show higher detection accuracy with fewer false alarms, improving leak detection. Zhang et al. (2023) [15], consider using a pseudo-Siamese convolutional neural network (PCNN) to detect leaks in water distribution systems (WDS) using ground acoustic signals. Handcrafted features and deep representations are combined, including Mel Frequency Cepstral Coefficients (MFCC) [16, 17]. The results show that the optimized PCNN model achieves an accuracy of 99.70%, demonstrating the effectiveness of this combination. This approach can improve the development of intelligent leak detection equipment.

Consequently, Koutsyiannis (2012) [18] argues that traditional methods for water management are inadequate due to the non-linearity of hydrosystems and their inability to handle future uncertainty. Linear and dynamic methods are insufficient, and stochastic extensions oversimplify systems. Therefore, traditional deterministic methods are not sufficient to face the complexity and variability of hydraulic systems and leak detection due to the number of variables involved in the process. Most studies do not adequately integrate advanced artificial intelligence (AI) and combinatorial optimization techniques. Although some continuous monitoring systems, such as that of Yang & Zhao (2020) [1], have been proposed, they face high false alarm rates that limit their effectiveness. Few studies have integrated multiple advanced techniques such as the Kalman filter, BiLSTM, and Monte Carlo dropout to improve accuracy and reduce uncertainty. Furthermore, the literature lacks a comprehensive evaluation of the spectral and temporal characteristics of pressure and flow signals to detect disturbances caused by leaks in real aqueduct systems. A comprehensive approach combining Kalman filter, BiLSTM, and Monte Carlo dropout is proposed to improve the accuracy of leak detection and reduce false alarms. A detailed analysis of the spectral and temporal characteristics of the pressure and flow signals will be performed, using the wavelet transform, to identify specific disturbances associated with leaks. Additionally, combinatorial optimization algorithms, such as minimum entropy deconvolution and attention mechanisms, will be implemented to improve the accuracy of leak identification and localization. The integration of IoT devices will allow real-time monitoring of critical variables of the hydraulic system, facilitating early and accurate detection of leaks. The validation of the model will be carried out in real environments, such as Sector III of the EAAB in Bethlehem, through exhaustive tests to verify the stationarity of the series and the robustness of the proposed approach.

## 2. Time Series Analysis: Pressure and Flow

The analysis of the behavior of pressure and flow signals for the detection of leaks in hydraulic systems is influenced by various variables. These include distortions caused by calibration processes, in situ conditions, intrinsic sensor noise, as well as aleatory and epistemic model uncertainty. Therefore, Thu et al. (2023) [19] stated that it is essential to determine the degree of impact that these conditions can have on the signals. The objective of characterizing the signals in statistical and spectral terms is to establish the independence, correlation, or stationarity of the time series, allowing the signal to be approached with a statistical approach appropriate to its behavior. This involves understanding and correctly modeling the statistical and spectral characteristics of the signals to develop effective leak detection and analysis strategies in hydraulic systems. The data used in this study were provided by the Aqueduct Service Division Headquarters Zone 3 of the Bogotá Aqueduct and Sewer Company (EAAB). The EAAB provided the calibrated hydraulic model of Zone 3 (@ WaterGEMS), as well as flow and pressure data from the different hydraulic districts. In addition, heat maps of damage to the networks corresponding to the year 2023 were included for the Hydraulic Districts of Zone 3. In particular, for District 3 (Belén).

Figure 1 illustrates the monthly average pressures for the year 2022 in Sector III of the EAAB in Belén. A diurnal variation in pressures is observed, with a general tendency for pressure to decrease during the night hours and a gradual increase throughout the day. This pattern remains consistent throughout the different months, although there are small variations in the magnitude of the pressures during the year. Notably, there is a decrease in pressure around 11:00 AM, especially in September. However, the highest pressures of the year were recorded in February around 4:00 AM, due to low consumption at that time. This variability in pressures is influenced by demand, the physical condition of the pipes, and the appearance of leaks in the hydraulic system.

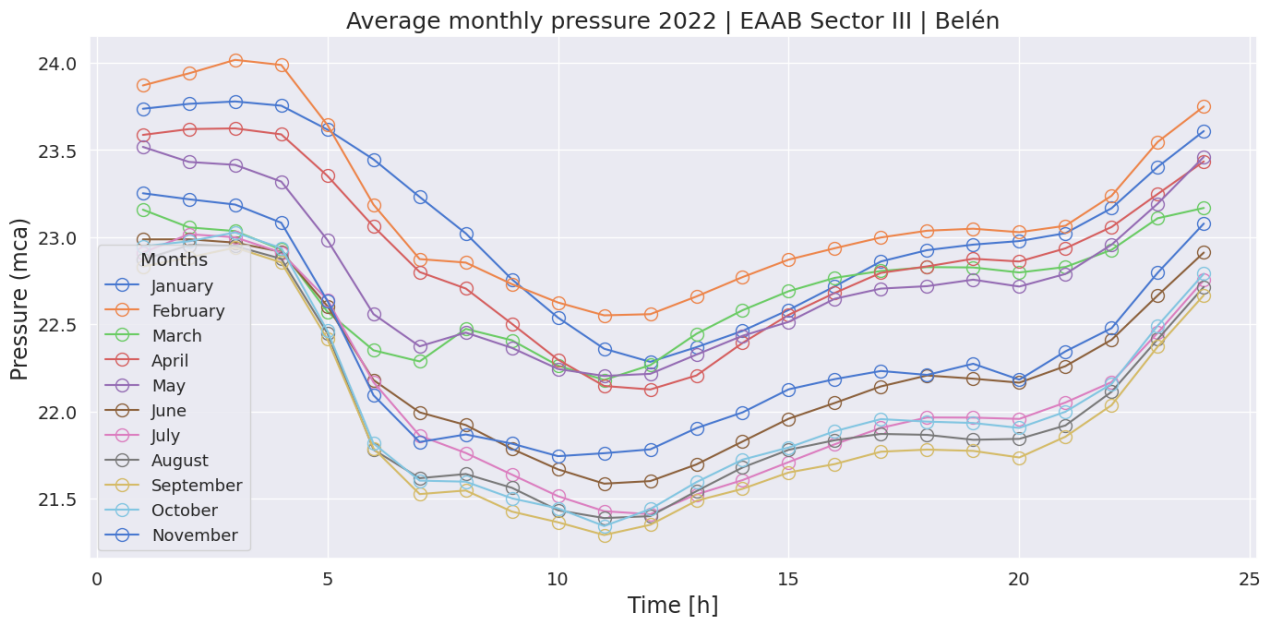


Figure 1. Average monthly pressure 2022 Sector III - Belén

On the other hand, Figure 2 depicts the average monthly water flow in Sector III of the EAAB in Belén during the year 2022. The data reflect a significant diurnal behavior, with a drastic increase in flow from the first hours of the morning, reaching a maximum around 11:30 AM. This pattern is repeated consistently throughout the different months, indicating stable water consumption in the Belén hydraulic district. After the peak, the flow gradually decreases and remains relatively stable until 9:00 PM, at which time demand decreases noticeably.

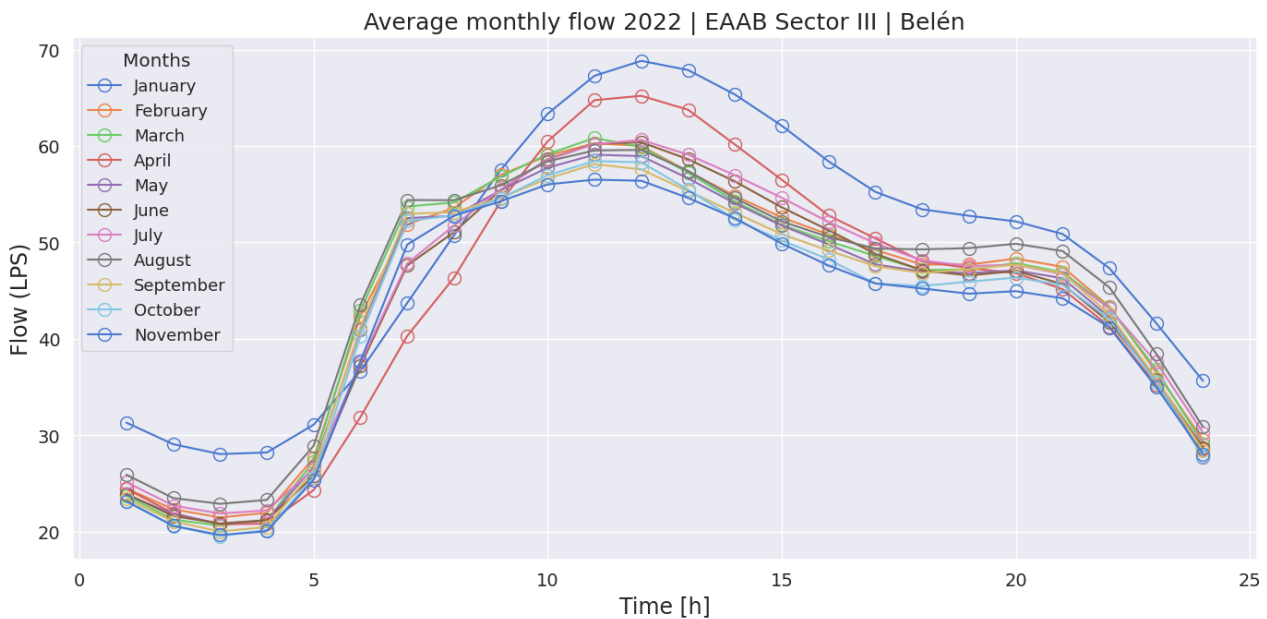


Figure 2. Average monthly flow 2022 Sector III – Belén

### 3. Isolation Forest

With the information provided by the EAAB, the reported *network damages* were identified, classified into the following categories: burst pipe, valve damage, network damage to be discovered, low pressure, and damage to be located by geophony. Using this information, the input data set was constructed. The response was classified in a binary manner, indicating a leak with a 1 and the absence of a leak with a 0. Therefore, the pressure and flow data were normalized by transforming the signal values to a standard range. This normalization process is crucial for the machine learning stage of the neural network as it prevents bias toward larger-scale values. In Python, the *MinMaxScaler* tool was used to fit the data to a range between 0 and 1. Figure 3 illustrates the time series of normalized pressure (mca) and

flow (LPS) data for Sector III of the EAAB in Belén. This series covers a period of 11 months and presents cyclical variations in both pressure and flow, suggesting a periodic behavior influenced by daily demand. Recurrent peaks and subpeaks are observed, with pressure and flow oscillating in a synchronous but inversely proportional manner at various time intervals. For example, when the flow rate increases, the pressure tends to decrease, due to the supply and demand dynamics of the hydraulic system. Significant increases in flow occur during daylight hours, influenced by the consumption habits of users.

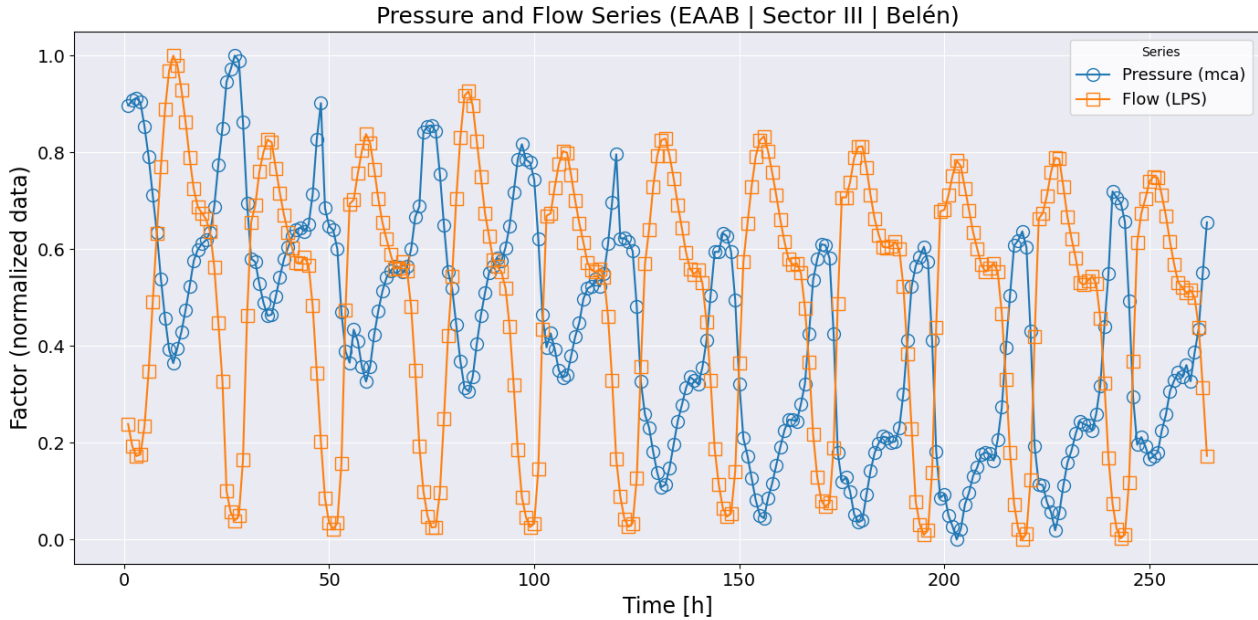


Figure 3. Normalized data: Pressure and flow Sector III - Belén

The first 5 normalized data are presented in Table 1.

Table 1. Normalization of pressure and flow data: Sector III - Belén

Time (s)	Pressure (mca)	Flow (LPS)	Leak=1	No Leak=0
1	0.897	0.237	1	
2	0.907	0.193	1	
3	0.912	0.172	1	
4	0.904	0.175	0	
5	0.853	0.234	1	

To detect anomalies in the pressure and flow series, the Isolation Forest method was used. This technique is used to identify anomalies in unlabeled data, detecting outliers in the time series. Isolation Forest constructs multiple isolation trees by recursively partitioning the pressure and flow data until each point is isolated. The anomaly score for data  $x$  is calculated as the average depth of the partition in which  $x$  is isolated via isolation trees. The shallower the partition, the greater the likelihood that  $x$  is an anomaly. In this way, the data set of normalized pressures and flows associated with network damage was integrated into the anomaly dataset. This data set established the baseline of labeled input data for the BiLSTM-Monte Carlo Dropout model. Figure 4 depicts the normalized time series of pressure and flow, represented by the blue and orange lines, respectively.

A periodic pattern is observed in both series, with regular fluctuations over time. Additionally, green dots indicate anomalies detected in the pressure data, while red dots indicate anomalies detected in the flow data. These anomalies represent points where the time series deviates significantly from the expected normal pattern. To predict the behavior of pressure and flow over time, an artificial neural network (ANN) is established. Zahran et al. (2020) [20] stated that it is possible to detect wave anomalies produced by leaks through strategic monitoring of the hydraulic network in a real system. A. The input data ( $X$ ) comprises the Hour and Month columns, while the outputs ( $y$ ) are the target variables Flow (LPS, liters per second) and Pressure (mca, meters of water column).

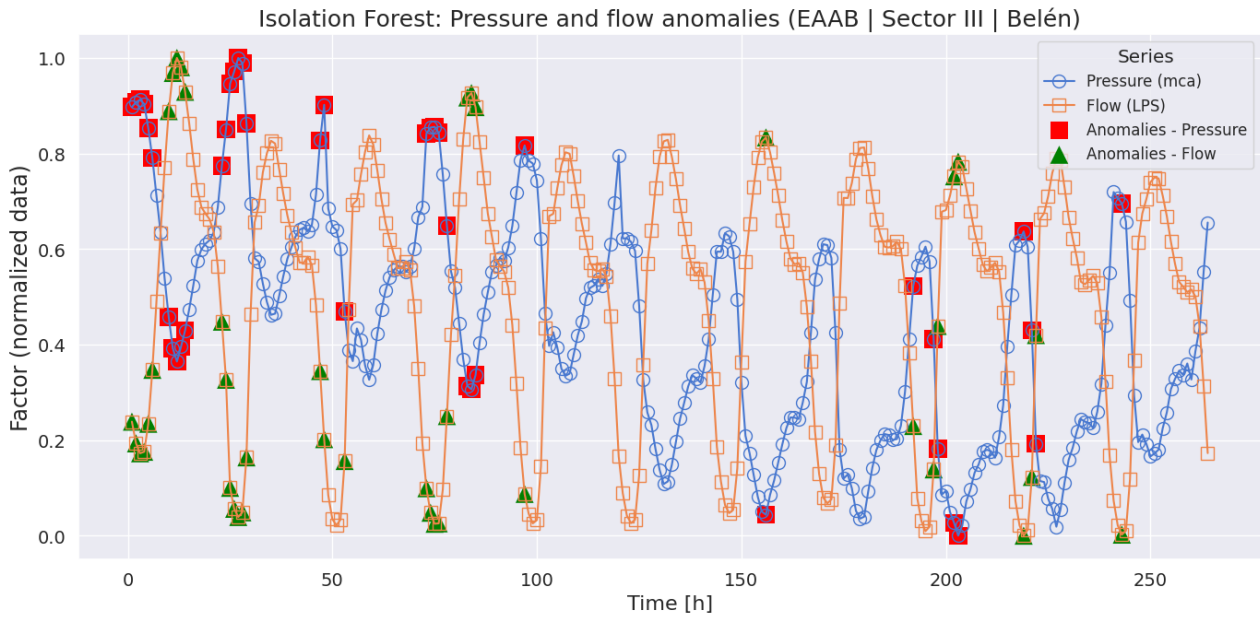


Figure 4. Isolation Forest: Pressure and flow anomalies Sector III - Belén

#### 4. Autocorrelation: EAAB Sector III-Belén

To identify the existence of patterns in pressure and flow data over time, the autocorrelation function is used to detect the presence of trends or seasonal cycles. The autocorrelation function for the time series  $X_t$  is defined as the correlation between  $X_t$  and  $X_{t+k}$ , where  $k$  is the number of lags. Therefore, the autocorrelation at lag  $k$  is given by:

$$\rho_k = \frac{\sum_{t=1}^{N-k} (X_t - \bar{X})(X_{t+k} - \bar{X})}{\sum_{t=1}^{N-k} (X_t - \bar{X})^2} \tag{1}$$

where  $N$  represents the total number of observations,  $X_t$  is the value of the series at time  $t$ ,  $\bar{X}$  is the mean of the series, and  $\rho_k$  is the autocorrelation coefficient at lag  $k$ . In this way.

The autocorrelation function (ACF) and partial autocorrelation function (PACF) for the pressure data in Sector III of the EAAB in Belén are presented in Figure 5. The autocorrelation function measures the correlation between the pressure time series and its lagged values at different time periods. It is observed that the first lags have positive and significant autocorrelation values, followed by a gradual decrease until reaching 12 lags. This pattern indicates a positive correlation between pressure values in nearby periods, suggesting that current pressure values are influenced by recent values.

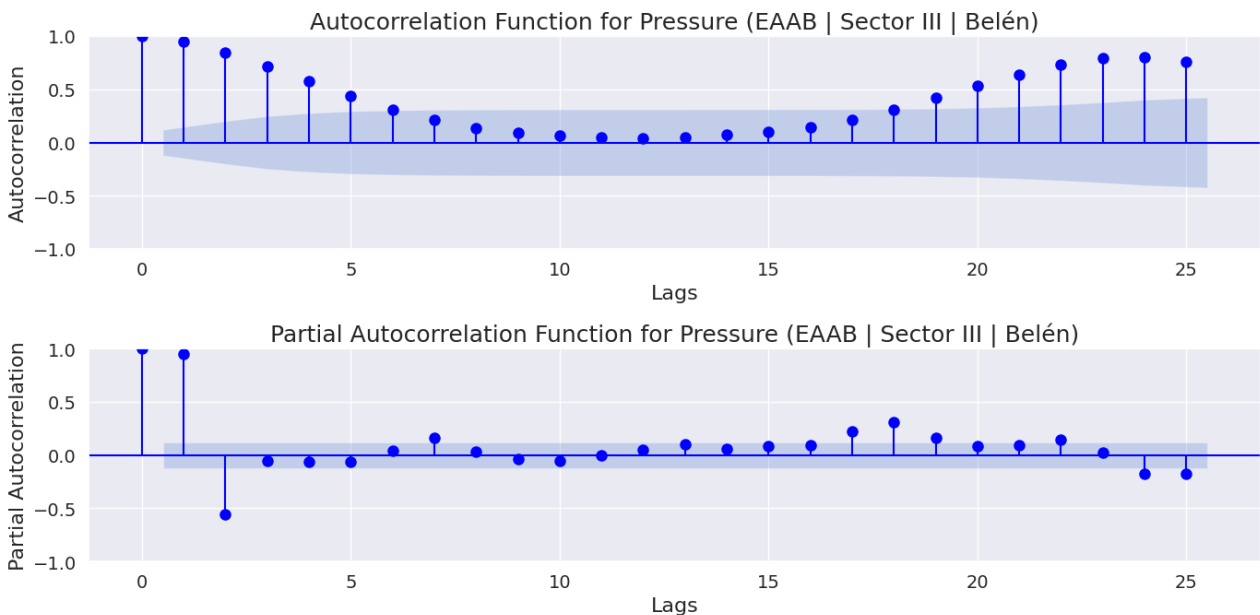


Figure 5. Autocorrelation function for pressure (EAAB | Sector III | Belén)

The gradual decrease and crossing of the 95% confidence line towards negative values indicate long-term memory loss, a common effect in time series where current observations depend on a limited number of past observations. Consequently, the pattern of the series suggests a temporal dependence in the pressure data, although the influence of past values decreases with time. Wu et al. (2018) [21], in effect, WDS data are spatially correlated time series. Likewise, the points outside the blue shadow, for lags between 0 and 6 and between 17 and 25, indicate that the autocorrelation is significantly different from zero, establishing a significant correlation between the values of the time series and their lags at those points. On the other hand, for points within the blue shade, the correlation is considered not significantly different from zero and can be attributed to some random component.

The second graph (PACF) for pressure depicts the correlation between the time series and its lags, eliminating the effect of intermediate lags. The first lags also present significant values of partial autocorrelation, especially the first lag, which confirms the short-term dependence observed in the ACF. The evolution of the series towards values close to zero indicates that most of the dependence in the time series can be explained by a few lags. In this sense, the time series depicts a pattern that suggests the possible existence of stationarity in terms of mean and variance, with a less significant long-term effect. Therefore, the subsequent lags suggest that the pressure data may be stationary since its statistical properties do not change with time. Figure 6 illustrates the correlation between the flow rate values and their own values at different delays. It is observed that the first delays (0-4) have positive and significant autocorrelation values, which indicates a significant correlation between flow values in close periods in time. As the number of lags increases, autocorrelation gradually decreases, although some significant values persist until approximately lag 15, establishing a short-term memory in the flow data, where current values are influenced by recent values. The existence of values outside the confidence interval (blue shadow) supports the presence of significant time dependence. Points below zero indicate negative autocorrelation, suggesting that the time series tends to oscillate around its mean. That is, a high flow rate at a given delay can be followed by a low flow rate at the next delay, creating a cyclical pattern. Therefore, the flow time series exhibits seasonality due to the identified periodic cycles. The stationarity of the time series is crucial for the construction of models that capture the dynamics implicit in the hydraulic system. In Sector III of the EAAB in Belén, the negative autocorrelation observed at certain lags may suggest that the flow experiences periodic or cyclical fluctuations, possibly related to demand patterns, where demand peaks are followed by periods of lower consumption.

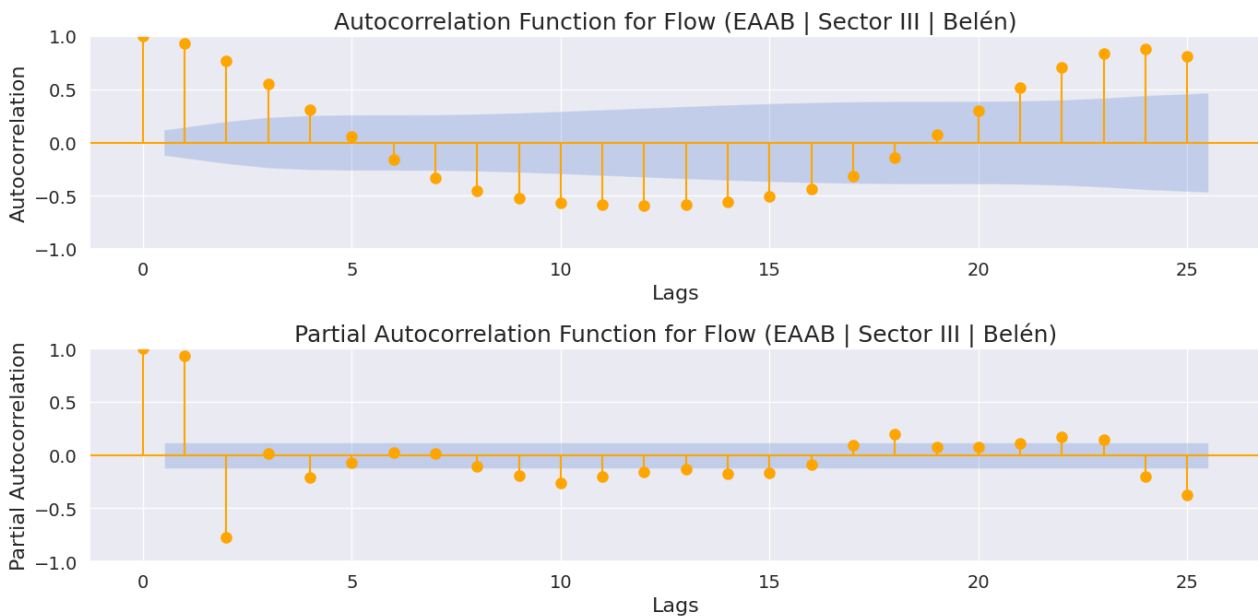


Figure 6. Autocorrelation function for flow (EAAB | Sector III | Belén)

### 5. Dickey-Fuller Test

To evaluate the presence of unit roots in the pressure and flow data, the Augmented Dickey-Fuller (ADF) test was used to determine if the pressure and flow series are stationary. If the series are stationary, it means that both the mean and the variance remain constant over time. In other words, for different instances of time, the same distribution occurs. The ADF model is defined by:

$$\Delta y_t = \alpha + \beta t + \gamma y_{t-1} + \delta \Delta y_{t-1} + \dots + \delta \Delta y_{t-p+1} + \varepsilon_t \tag{2}$$

where  $\Delta y_t$  is the first difference of the time series,  $\alpha$  is the constant term,  $\beta t$  is the term trend, and  $\gamma$  is the lag coefficient of the series being tested for the presence of a root unitary. The ADF test focuses on the null hypothesis that  $\gamma = 0$ , indicating the presence of a unit root and, therefore, non-stationarity in the time series. Therefore, the null hypothesis  $H_0: \gamma = 0$ , indicates that the series has a unit root. However, the alternative hypothesis  $H_1: \gamma < 0$ , suggests that the series

does not have a unit root and is stationary. Table 2 presents the results of the Dickey-Fuller test used to determine the stationarity of the pressure (mca) and flow (LPS) time series in Sector III. The existence of a unit root in both series was evaluated, which would indicate the non-stationarity of the series. The significance levels of 1%, 5% and 10% were established to compare with the test statistic obtained. For the pressure series, the test statistic is -3.892. When comparing this value with the critical values, it is observed that the test statistic is lower in absolute terms than all the critical values. This means that the null hypothesis of the presence of a unit root is rejected at the 1%, 5%, and 10% levels of significance. Therefore, it is concluded that the pressure series is stationary. Stationarity implies that the statistical properties of the pressure time series do not change over time, making the pressure and flow data viable, once normalized, for use in building the BiLSTM-Monte Carlo Dropout model

**Table 2. Dickey-Fuller test for flow and pressure series: Sector III**

Variable	Test Statistic	Critical Value (1%)	Critical Value (5%)	Critical Value (10%)
Pressure (mca)	-3.892	-3.452	-2.871	-2.571
Flow (LPS)	-4.321	-3.452	-2.871	-2.571

For the flow time series, the test statistic was -4.321. Compared to the critical values of -3.452 (1%), -2.871 (5%), and -2.571 (10%), it is evident that the null hypothesis of a unit root presence can be rejected at the 1%, 5%, and 10% significance levels. Therefore, the flow series is stationary. Consequently, it is concluded that both time series, flow and pressure, are stationary according to the results of the Dickey-Fuller test. This significantly contributes to the statistical analysis and predictive modeling in the detection of potential leaks in the hydraulic system. In the Principal Component Analysis (PCA) carried out for the pressure and flow data from Sector III of the EAAB in Belén, the dimensionality of the observed data was transformed into a new set of uncorrelated variables, in order to retain the greatest part of the variability implicit in the data measured in situ. In this way, Principal Component 1 (PC1) represents the direction in which the data depicts the greatest variation, which is shown on the horizontal axis. For Principal Component 2 (CP2), located on the vertical axis, the distribution of the data can be observed along this second component, where the dispersion of the points reflects the variability present in the data. This distribution is illustrated in Figure 7. Using the K-Means algorithm, clusters were grouped for the data from Sector III of the EAAB in Belén, projected in the space of the first two principal components, CP1 and CP2. Points that share similar characteristics are grouped in Cluster 0 (Red), just as in Cluster 1 (Green) and Cluster 2 (Blue). Shao et al. (2019) [22] indicated the clustering method uses cosine distance to evaluate the dissimilarity between data from multiple signals. Sun et al. (2022) [23] proposed SALICT, a cluster-based leak detection model, which only needs WDN (Water Distribution Network) flow data. The graph on the right illustrates three defined regions. This segregation helps detect leaks by segmenting the water distribution system into regions for individual analysis, improving efficiency and facilitating the detection of anomalies in pressure and flow signals, supporting data-driven decisions.

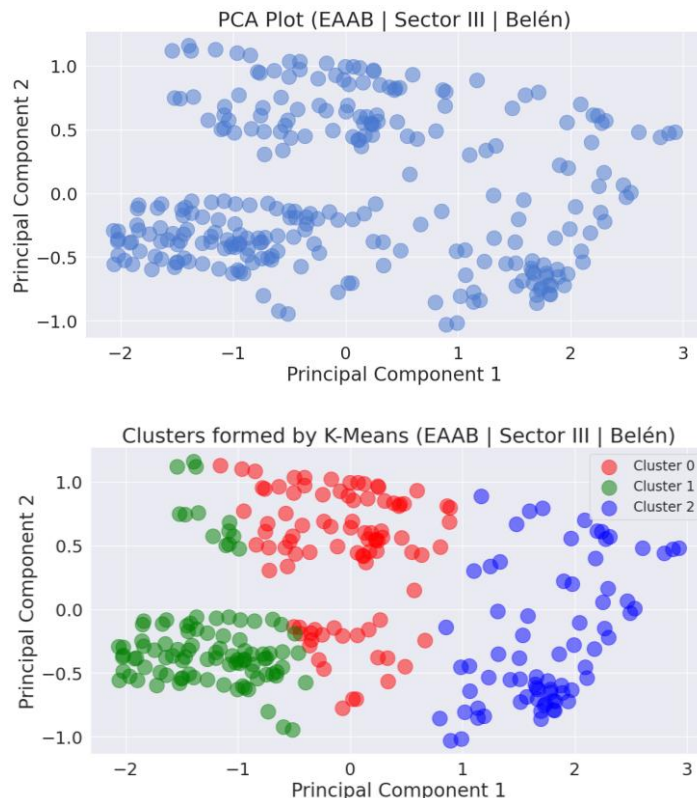


**Figure 7. Components - Clusters - K-Means (EAAB | Sector III | Belén)**

## 6. Hurst Exponent: Pressure and flow

This study analyzed the behavior of autocorrelation and long-term memory in pressure and flow series by implementing the Hurst Exponent. The objective of this analysis was to determine the temporal structure of the series. The Hurst Exponent, denoted as  $H$ , is defined for a time series  $X(t)$  as follows:

$$H = \lim_{n \rightarrow \infty} E \left[ \left( \frac{S(n)}{n} \right)^H \right] \quad (3)$$

where  $E[\cdot]$  represents the expected value,  $S(n)$  is the accumulated sum of the differences between the time series values at different times, and  $n$  is the size of the time window. The exponent Hurst provides information on autocorrelation and persistence of the time series. A value of  $H = 0.5$  indicates random behavior (diffusion process).  $H$  values  $> 0.5$  suggest positive autocorrelation and long-term persistence, while  $H$  values  $< 0.5$  indicate low correlation. Analysis of the pressure and flow time series revealed significant details about their dynamic characteristics.

The Hurst exponent for pressure was measured to be approximately 0.2545, indicating an antipersistent phenomenon where oscillations are prominent and long-term correlation is poor. This finding suggests that changes in pressure are marked by oscillatory fluctuations that do not show pronounced continuity over time. On the other hand, the Hurst exponent for the flow was even lower, approximately 0.1379, indicating more abrupt changes influenced by recent variations that may be in the opposite direction. This low exponent measure indicates a temporal structure where current flow variations are more influenced by immediate events and less by past states, reflecting a more volatile and less predictable dynamic compared to pressure.

To evaluate the presence of autocorrelation in both series and determine the relationship between the values over time, the Durbin-Watson test was applied. The results showed a Durbin-Watson statistic of 0.01873 for pressure and 0.02794 for flow. These values indicate a strong positive autocorrelation in both cases, suggesting that the current values are significantly influenced by their preceding values. In the case of pressure, this positive autocorrelation implies notable persistence in observed trends and patterns, where current changes consistently reflect past variations. Similarly, for flow, positive autocorrelation underscores a consistency in temporal fluctuations, with recent conditions significantly influencing current conditions.

## 7. Spectral Analysis: EAAB Sector III-Belén

To transform the pressure and flow signals from the time domain to the time-frequency domain, the signals are segmented. Subsequently, to reduce the spectral distortion, a window function is applied, which is affected by the Short-Time Fourier Transform (STFT). If  $x(t)$  is the pressure signal and  $w(t)$  is the window function, the STFT is defined as:

$$STFT\{x(t)\}(\tau, \omega) = \int x(t)w(t - \tau)e^{-j\omega t} dt \quad (4)$$

where  $\tau$  is the temporal displacement of the segment and  $\omega$  is the angular frequency. Given the above, it is possible to construct the spectrogram, which represents the square of the magnitude of the STFT, generating a two-dimensional representation of the signal power spectrum and showing the evolution of the signal over time.

Thus, the  $P$  spectrogram is calculated as:

$$P(\tau, \omega) = |STFT\{x(t)\}(\tau, \omega)|^2 \quad (5)$$

Consequently, spectral analysis focused on the identification of anomalies, such as leaks, from pressure and flow signals constitutes a significant contribution to the management of hydraulic systems. This approach seeks to establish the *spectral imprint* of leaks, that is, the specific frequency at which they occur. By identifying and separating this frequency from the general spectrum of pressure and flow signals, we contribute to the energy characterization of the hydraulic system. Figure 8 presents the pressure spectrogram (mca) for Sector III of the EAAB in Belén, indicating the variation in the intensity of the pressure signal frequencies over time. This makes it possible to identify variations in frequency and intensity that may be associated with disturbances caused by leaks. The pressure spectrogram presents different color bands that show how the intensity of the frequencies varies with time. It is observed that the majority of the energy of the pressure signal is concentrated at low frequencies, around 0.1 to 0.3 Hz. This concentration indicates that the variations in pressure are more significant at these frequencies, which agrees with the behavior of the pressure hydraulic systems. The white circles in the spectrogram represent the detected leaks, which occur at specific frequencies, around 0.25 Hz, and at specific moments in time.

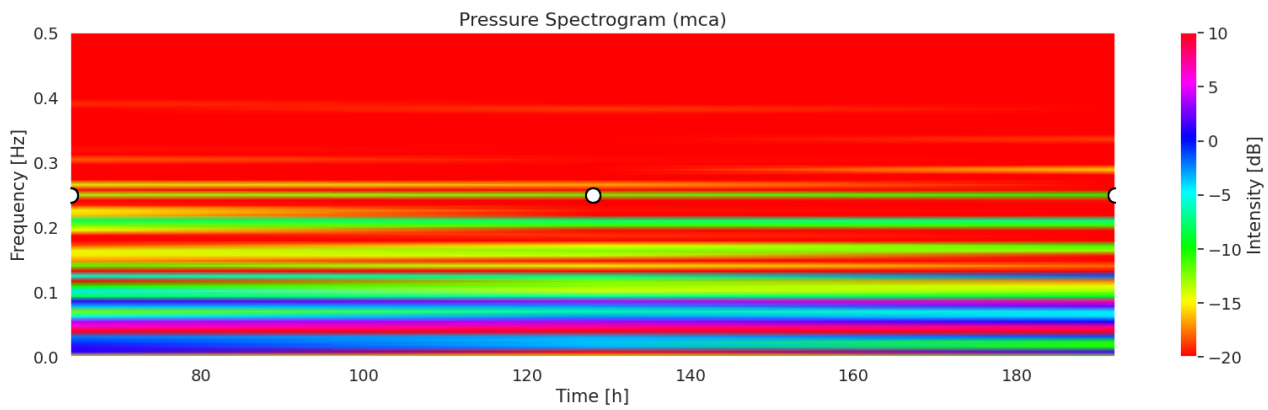


**Figure 8. Pressure spectrogram (mca) | EAAB | Sector III | Belén**

The identification of these frequencies associated with leaks is crucial for real-time monitoring of the system, as it allows inspections and maintenance interventions to be focused on the frequency ranges where spectral distortions caused by leaks are most likely to occur. The signal intensity, measured in decibels (dB), is represented in a range in which red indicates the highest intensity and blue indicates the lowest. In the spectrogram shown in Figure 8, it is observed that most of the pressure signal has a high intensity (in red), which suggests a strong presence of energy in the low frequencies. A decrease in intensity is identified around frequencies of 0.25 Hz, which could be related to the pressure disturbance in the system caused by these leaks (white circles). High intensity at certain frequencies could indicate areas of the system that require greater attention and real-time monitoring, while variations in intensity can provide clues about leak dynamics and their effects on the system. This high intensity at the 0.25 Hz frequency implies that leaks generate significant changes in system pressure. This entails the need to structure intelligent, autonomous, and resilient hydraulic systems, capable of reacting to hydraulic eventualities autonomously, based on learning patterns.

Figure 9 presents the flow spectrogram (LPS) corresponding to Sector III of the Bogotá Aqueduct and Sewer Company (EAAB) in the Belén area. This graph displays the variation in intensity of different frequencies of the flow signal over time, with a horizontal axis representing time in hours and a vertical axis showing frequency in hertz (Hz).

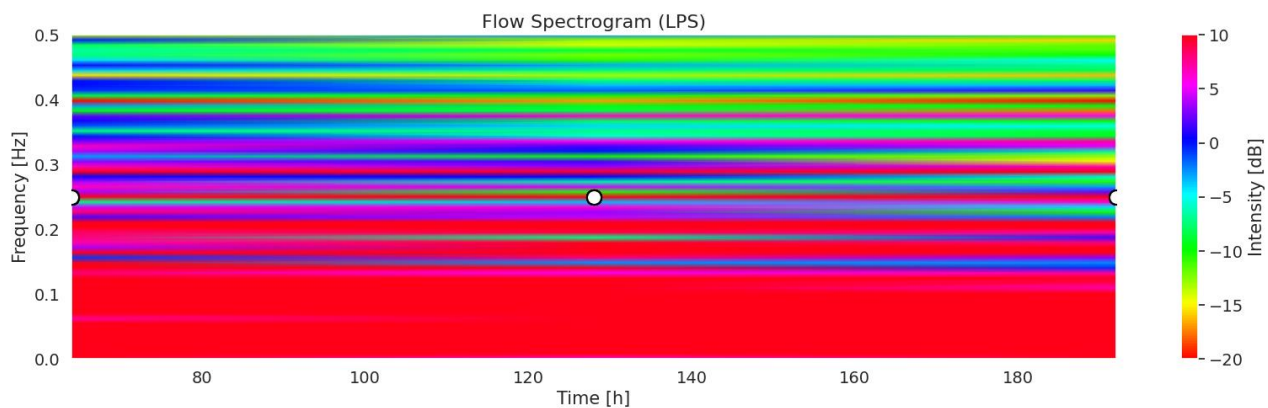


**Figure 9. Flow spectrogram (LPS) | EAAB | Sector III | Belén**

The spectrogram allows flow disturbances caused by leaks to be identified and analyzed. In the figure, you can see colored bands that indicate the intensity of the frequencies, where warmer colors (red) represent greater intensity. Specifically, a prominent red band can be noted around the 0.25 Hz frequency, suggesting significant energy at this frequency, attributable to leakage. The white circles in the graph indicate the specific frequencies at which significant disturbances are detected. These markers highlight the presence of leaks and the energy associated with these disturbances. As in the pressure analysis, leaks show a notable concentration at the 0.25 Hz frequency, reinforcing the idea that this frequency is a critical indicator of the presence of leaks in the water distribution system.

This indicates that leak-related flow variations have a significant energy (*spectral imprint*) at this frequency. From the normalized data for pressure (mca), the Wavelet spectrogram was constructed (Figure 10), which provides a detailed representation of the variation of the energy of the pressure signals at different scales and over time, to detect transient events such as leaks in the hydraulic system. White circles in the spectrogram represent leak detections. The concentration of energy at certain scales indicates the presence of variations in pressure at those specific frequencies. A significant concentration of energy is observed at the low scales, indicating high-frequency variations in pressure.

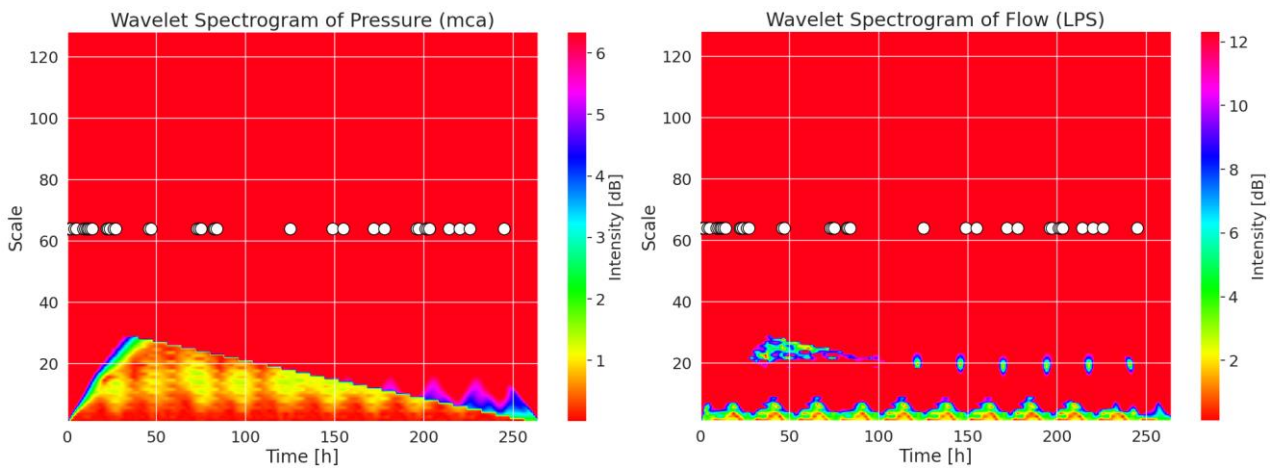


Figure 10. Wavelet spectrogram: Pressure - Flow | EAAB | Sector III | Belén

The yellow triangle shown in the left graph indicates a significant concentration of energy in the lower scales (*higher frequencies*) at the beginning of the analyzed time period. This area of high intensity suggests that there are rapid and significant variations in water pressure, especially at  $t = 40$  h. Afterward, the energy begins to gradually decrease. In addition, energy peaks (magenta color) associated with the appearance of leaks (indicated by the white circles) are observed at  $t = 210$  h,  $t = 240$  h, and  $t = 250$  h.

The graph on the right provides a detailed view of the energetic variability of the flow signal at various time scales and over time. Similar to the pressure signal, a high concentration of energy is observed in the lower scales (higher frequencies) during the first 50 hours, represented by the yellow and green triangle at the bottom left of the figure, with a scale of approximately 30. This high energy at high frequencies suggests rapid and significant flow variations in this period, attributable to changes in user demand or the possible appearance of leaks in the system.

As time progresses, the energy at these frequencies decreases, indicating a stabilization of the flow in energetic terms. The white circles, which indicate the presence of leaks, are mainly scattered between scales 65 and 70, suggesting that these leaks are associated with low-frequency variations in the flow. This pattern of leak detection at low frequencies may be indicative of events that have a prolonged impact on the distribution system, such as leaks that develop gradually.

For scale 20, spontaneous energy dissipation with an approximate value of 6 dB are observed at times  $t = 120$  h,  $t = 148$  h,  $t = 170$  h,  $t = 190$  h,  $t = 220$  h and  $t = 240$  h. These energetic peaks are directly associated with the appearance of leaks, indicated by the white circles in the spectrogram. This methodology allows real-time energy monitoring of the system from dynamic spectrograms, facilitating the detection of energy anomalies caused by transient events, such as leaks.

### 8. Material and Methods

The proposed methodology for leak detection in urban hydraulic systems employs an integrated approach using the K-BiLSTM-MC model (Figure 11). Initially, pressure and flow data are captured and downloaded, followed by statistical analysis and normalization of the sequences. Temporal cross-validation is applied to ensure the robustness of the data. Subsequently, the Kalman filter is implemented to stabilize the pressure and flow signals, improving the accuracy and prediction ability.

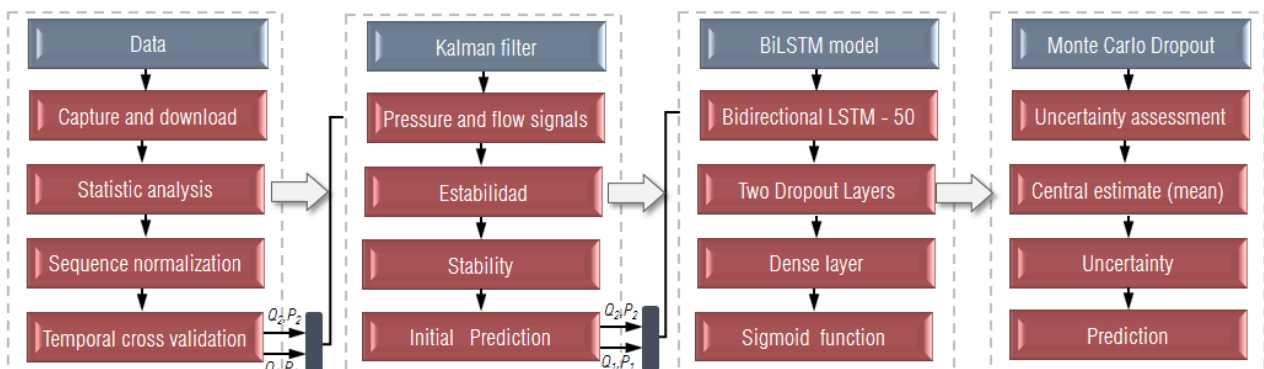


Figure 11. K-BiLSTM-MC Model methodology for leak detection in urban hydraulic systems

These filtered signals are fed into a bidirectional BiLSTM model with 50 units, which consists of two Dropout layers and a dense layer with a *sigmoid* activation function to generate the predictions. Finally, the Monte Carlo Dropout method is used to evaluate the uncertainty in the predictions, providing a central estimate (mean) and standard deviation. This comprehensive approach enables accurate and reliable leak detection, optimizing the monitoring and management of urban hydraulic systems.

### 9. Kalman Filter and Model K-BiLSTM-MC

To eliminate possible noise and random fluctuations, the Kalman filter was adopted to improve the ability of the recurrent neural model to learn meaningful patterns. In terms of stability, the Kalman filter contributes to increasing the accuracy during the implementation of the BiLSTM (Bidirectional Long Short-Term Memory) model in the training and validation stages, which is reflected in the statistical control metrics adopted. Additionally, by filtering the data before applying the neural model, the possibility of overfitting during learning is reduced, allowing the recurrent model to respond more effectively to new data sets. For the Kalman filter the state of the system at time  $k$  is denoted as  $x_k$ , and can be represented by a linear state space model, thus:

$$x_k = A \cdot x_{k-1} + B u_k - w_k \tag{6}$$

where  $A$  is the state transition matrix that models the evolution of the system.  $B$  is the matrix control that relates the control input  $u_k$  to the change in the state of the system.  $w_k$  is the process noise with zero mean. Figure 12 presents the application of the Kalman filter to the pressure data (mca) for Sector III of the EAAB in Belén. The original pressure measurements are observed (in blue) and the pressures are filtered by the Kalman filter (in red). The pressures in Sector III of the EAAB in Belén present a general trend with cyclical variations over time. The objective of applying the Kalman filter is to smooth the pressure signal, eliminating noise and allowing a better interpretation of the trends.

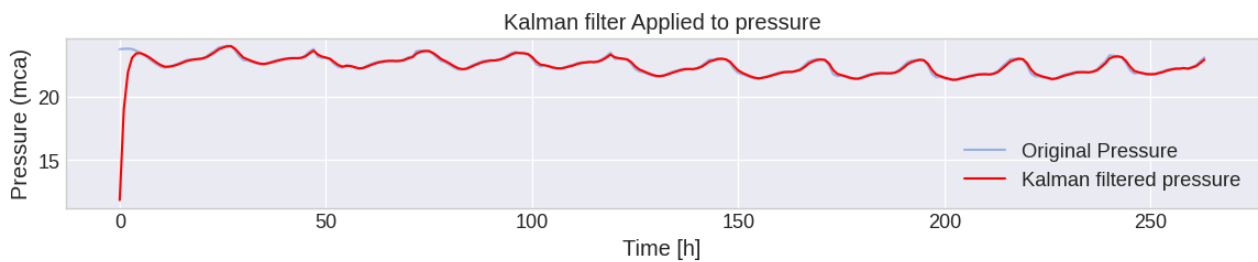


Figure 12. Kalman filter: Pressure | EAAB | Sector III | Belén

Daily pressure fluctuations are more noticeable in the filtered series, suggesting the existence of repetitive patterns associated with daily consumption and disturbances in the distribution network. The advantage of this filter lies in its smoothing capacity, since it maintains the peaks and subpeaks without eliminating extreme data, such as abrupt jumps produced by leaks in the system

For the flow rate, Figure 13 presents the smoothing of the fluctuations. The original flow series is represented by the blue curve, while the orange curve represents the signal filtered through the Kalman filter. The flow peaks observed indicate the moments of greatest demand for water by users. To detect patterns in the time series, the BiLSTM model was established, which analyzes the sequences of pressure and flow signals in both directions, allowing patterns dependent on past and future information to be identified. Sequences of features and labels with a size equal to 10 are used. The resulting sequences  $(X,y)$  are divided into training and test sets, setting 20% of the input data set for the test set. The BiLSTM model is configured as a sequential network consisting of two bidirectional LSTM layers, each with 50 units. The first LSTM (Long Short-Term Memory) layer is designed to return complete sequences, allowing the next layer to also process sequences.

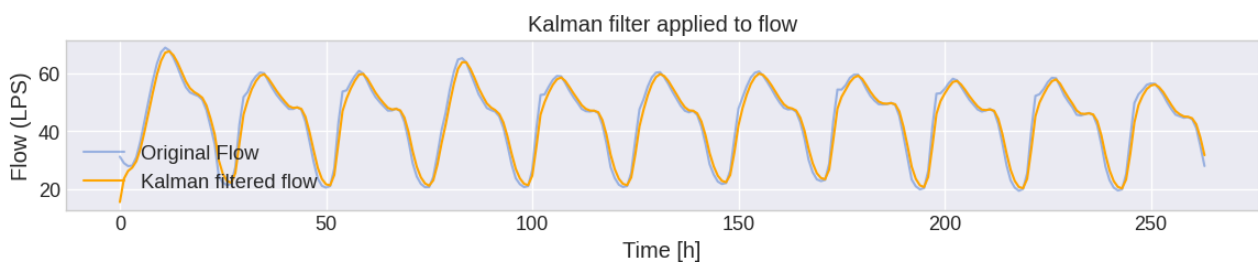


Figure 13. Kalman filter: Flow | EAAB | Sector III | Belén

Between each LSTM layer, Dropout is applied with a rate of 0.5, using Monte Carlo Dropout to regularize the model and capture uncertainty in the predictions. Finally, a dense layer with a *sigmoid* activation function generates the model output. The model is compiled with the *Adam* optimizer, using the MSE as the loss function and using the MAE as the accuracy metric to evaluate its performance.

For the flow rate, Figure 13 presents the application of the Kalman filter to the flow signal in a hydraulic system. The graph compares the original flow signal (blue line) and the filtered flow signal (orange line) over time, represented in hours on the horizontal axis and the flow in LPS on the vertical axis. The Kalman filter is used to reduce noise and unwanted fluctuations in the original signal, providing a smoother and more accurate estimate of the actual flow. It is observed that the filtered signal closely follows the trend of the original signal, but with greater smoothness, especially in the peaks and valleys of the flow oscillations. This noise reduction is critical to identifying and analyzing more consistent flow patterns, allowing for better detection of anomalies such as leaks. In addition, the implementation of the Kalman filter facilitates the monitoring and control of the hydraulic system, improving the precision in the measurement and analysis of flow signals in real time.

## 10. Model K-BiLSTM-Monte Carlo Dropout

The BiLSTM (bidirectional long short-term memory) architecture is a type of recurrent neural network (RNN) used to analyze temporal data sequences. In this study, pressure and flow signals were obtained from Sector III of the EAAB in Belén. The time series of pressure signals is represented by  $\{P_1, P_2, \dots, P_T\}$ , and the flow signals by  $\{Q_1, Q_2, \dots, Q_T\}$ , where T represents the number of time instants. Furthermore, for each instant of time, there is an associated label that indicates the presence or absence of leaks, represented by  $\{L_1, L_2, \dots, L_T\}$ , where  $L_t = 1$  if a leak is detected at instant t and  $L_t = 0$  if there are no leaks. A loss function is used to train the network; In this study, the binary cross-entropy function was adopted, which compares the network predictions with the actual leakage labels.

Through the training process, the network adjusts its weights and internal parameters to minimize the cost function and improve the model's prediction capacity in leak detection, based on pressure and flow signals over time. The LSTM establishes different memory units called memory cells, which are updated at each time step. For a one-way LSTM, the memory cell update at time t is calculated as follows:

$$i_t = \sigma(W_{xi}x_t + W_{hi}h_{t-1} + b_i) \quad (7)$$

$$f_t = \sigma(W_{xf}x_t + W_{hf}h_{t-1} + b_f) \quad (8)$$

$$o_t = \sigma(W_{xo}x_t + W_{ho}h_{t-1} + b_o) \quad (9)$$

Therefore,

$$g_t = \tanh(W_{xg}x_t + W_{hg}h_{t-1} + b_g) \quad (10)$$

LSTM output,

$$h_t = [\vec{h}_t; \overleftarrow{h}_t] \quad (11)$$

where  $[\cdot; \cdot]$  denotes the concatenation of vectors and  $\vec{h}_t, \overleftarrow{h}_t$  represents the outputs of the LSTM unidirectional at time t. The BiLSTM model analyzes the sequences of pressure and flow signals in both directions, allowing the identification of patterns dependent on past and future information. The algorithm uses sequences of features and labels with a size equal to 10. The resulting sequences (X, y) are divided into training and test sets, setting 20% of the input data set to the test set. The BiLSTM model is configured as a sequential network consisting of two bidirectional LSTM layers, each with 50 units. The first layer of LSTM is designed to return complete sequences, allowing the next layer to also process sequences. Between each LSTM layer, Dropout is applied with a rate of 0.5, using Monte Carlo Dropout to regularize the model and capture uncertainty in the predictions.

Finally, a dense layer with a *sigmoid* activation function generates the model output. The model is compiled with the *Adam* optimizer, using the MSE as the loss function and the MAE as the accuracy metric to evaluate its performance. Model training is performed for 200 epochs with a batch size of 64. Table 3 presents the results of training the BiLSTM model over the last five epochs, evaluating both loss and validation for the sets of training data (80%) and test data (20%). The loss values for the training data show reduced variability between 0.1002 and 0.0985, indicating that the loss remains low and stable. This suggests that the model can interpret the pattern of the training data. Furthermore, the accuracy of the model presents a tendency to remain high, confirming its effectiveness in interpreting the data. However, the lowest precision is observed at epoch 199, while in other epochs the precision remains at 0.8048. Validation loss values range between 0.1541 and 0.1563, suggesting that the model can generalize adequately and avoid overfitting. For

the validation data set (20%), the validation accuracy remains constant around 0.8048 and 0.8049, indicating that the model has consistent performance on the validation data. This demonstrates that the BiLSTM-Kalman-Monte Carlo Dropout model is effective in predicting pressures and flows in sector III of Belén, maintaining a low loss and mean absolute error in both training and validation.

**Table 3. K-BiLSTM-MC Model metrics and performance**

Epoch	Loss	Accuracy	MAE	Loss Validation	Accuracy Validation	MAE Validation
195	0.1002	0.8777	0.2003	0.1541	0.8049	0.2464
196	0.1003	0.8777	0.2037	0.1538	0.8048	0.2479
196	0.1003	0.8777	0.2037	0.1538	0.8048	0.2479
197	0.1016	0.8777	0.2004	0.1538	0.8048	0.2450
198	0.0968	0.8777	0.1893	0.1562	0.8048	0.2411
199	0.0985	0.8777	0.1878	0.1563	0.8048	0.2407

Figure 14 presents the plots of the model loss, mean absolute error (MAE), and validation metrics for the BiLSTM-Kalman-Monte Carlo Dropout model trained on EAAB Belén Sector III. The first graph presents the evolution of the model loss for both the training and validation sets over 200 epochs. It is observed that the training loss decreases continuously, indicating that the model improves its ability to fit the training data. The validation loss, although initially showing significant variations, gradually stabilizes and decreases, suggesting that the model is generalizing well without overfitting.

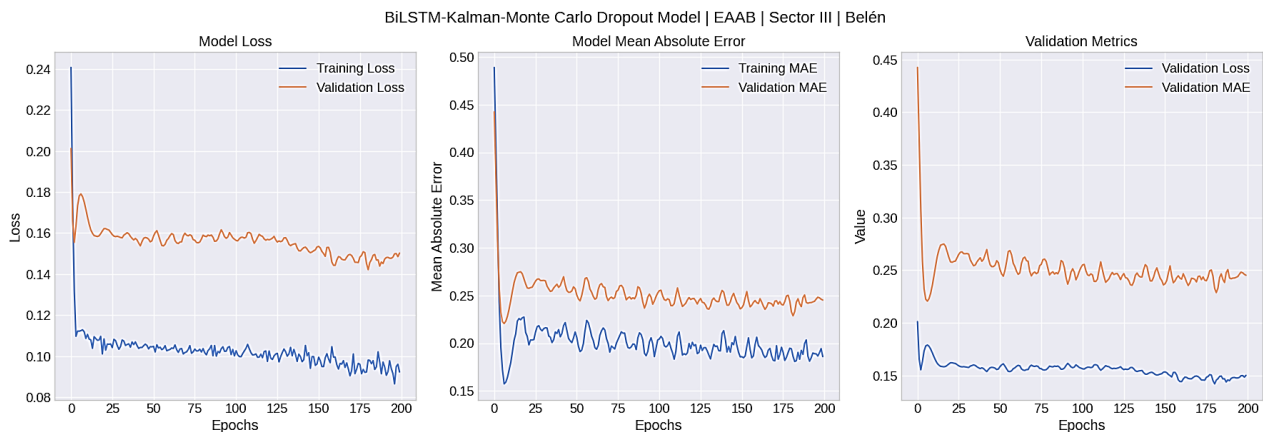


**Figure 14. Performance metrics: Pressure – Flow | EAAB | Sector III | Belén**

These fluctuations in the training and validation loss curves are typical characteristics of real data. The second graph illustrates the MAE for both training and validation. As with the loss, the MAE in the training set decreases steadily, indicating that the model improves its prediction accuracy over time, stabilizing around epoch 200. This was evidenced by creating 5 scenarios for different epochs until epoch 400. It was found that, after epoch 200, the model control metrics remained constant, indicating performance stability. In particular, for the validation MAE, the trend is decreasing, although with some fluctuations, which suggests that the model maintains an excellent generalization capacity. Furthermore, the third graph combines the validation loss and the validation MAE, showing that, although both metrics present fluctuations, they maintain a general downward trend. The model was tested with 185 unknown data, achieving an accuracy of 80.47%. This result suggests that the model has strong generalization ability, as it can apply the patterns learned during training to new data sets without incurring overfitting.

The ability to avoid overfitting is critical for predictive modeling, as it ensures that the model does not *overfit* specific training data and can effectively handle variations and new data in real-world scenarios.

### 11. Prediction and Uncertainty: EAAB Sector III-Belén

The model prediction process is carried out using the Monte Carlo Dropout algorithm to estimate the uncertainty in the predictions. First, a function is defined to perform multiple predictions (100 iterations) for each input data point. In each iteration, Dropout is activated in training mode, allowing the model to make different predictions due to the randomness induced by Dropout. These predictions are stored in a results matrix, which is then used to calculate both the average prediction and the uncertainty (standard deviation) for each data point. This allows us to obtain not only the most likely prediction but also a measure of the model's confidence in each prediction. Table 4 presents some results from the training set, showing both the model predictions and the corresponding uncertainties. For example, at time 39,

the pressure value is 22.870 mca and the flow rate is 52.587 LPS. The actual label indicates a leak (1), and the model correctly predicts this leak with a low uncertainty of 0.025. Likewise, at times 40 to 43, the actual labels are 0 (no leak) and the model adequately predicts the absence of leaks, with uncertainties ranging between 0.025 and 0.045.

**Table 4. Training results (BiLSTM-Monte Carlo Dropout)**

Time (h)	Pressure (mca)	Flow (LPS)	Real Label	Prediction (BiLSTM)	Uncertainty
39	22.870	52.587	1	1	0.025
40	22.936	50.818	0	0	0.027
41	22.997	49.210	0	0	0.005
42	23.036	47.707	0	0	0.004
43	23.048	47.691	0	0	0.045

Once the function is defined, it is applied to both the training and test sets to obtain the predictions and corresponding uncertainties. The resulting predictions are binarized by rounding them to 0 or 1 based on a threshold of 0.5, making it easy to interpret the results in terms of leakage (1) or no leakage (0). Furthermore, for better visualization, the input data (flow, pressure, and time) are denormalized using the inverse of the normalization process applied above. This allows the results to be interpreted in the original units. This approach not only provides accurate predictions but also incorporates an estimation of uncertainty, adding a layer of valuable information for making decisions based on the model predictions. Table 5 illustrates the results of the test set. It is observed that for time 193, the pressure is 22.831 mca and the flow rate is 23.397 LPS, with an actual label of 0 (no leak), and the model correctly predicts 0 with an uncertainty of 0.003. This low uncertainty suggests that the model is very confident in its prediction.

**Table 5. Test results (BiLSTM-Monte Carlo Dropout)**

Time (h)	Pressure (mca)	Flow (LPS)	Real Label	Prediction (BiLSTM)	Uncertainty
191	22.413	38.436	0	0	0.037
192	22.714	30.856	0	1	0.133
193	22.831	23.397	0	0	0.003
194	23.883	21.057	1	0	0.011
195	23.939	20.000	0	0	0.017

Figure 15 represents the distribution of uncertainties in the training and test sets. In the graph on the left, you can see the uncertainty boxes for both sets. The upper box, corresponding to the test set, illustrates that most of the uncertainties are concentrated in a low range, between 0.02 and 0.05, with some outliers reaching up to 0.20. These outliers, represented by black circles, indicate predictions with significantly larger uncertainties than the rest. Similarly, the lower box, corresponding to the training set, also depicts a concentration of uncertainties in a low range, between 0.01 and 0.04, with some outliers reaching up to 0.20. The graph on the right is a histogram showing the density of prediction uncertainties for both sets, along with a Gumbel fit. The histogram reveals that most prediction uncertainties are low, peaking around 0.02. The Gumbel fit curve, represented in red, indicates that the distribution of uncertainties follows a predictable trend. Together, these plots suggest that the model has high confidence in most of its predictions, although there are some predictions with higher uncertainties, especially in the test set. This provides a detailed insight into the stability and accuracy of the BiLSTM-Kalman-Monte Carlo Dropout model in leak detection in urban hydraulic systems.

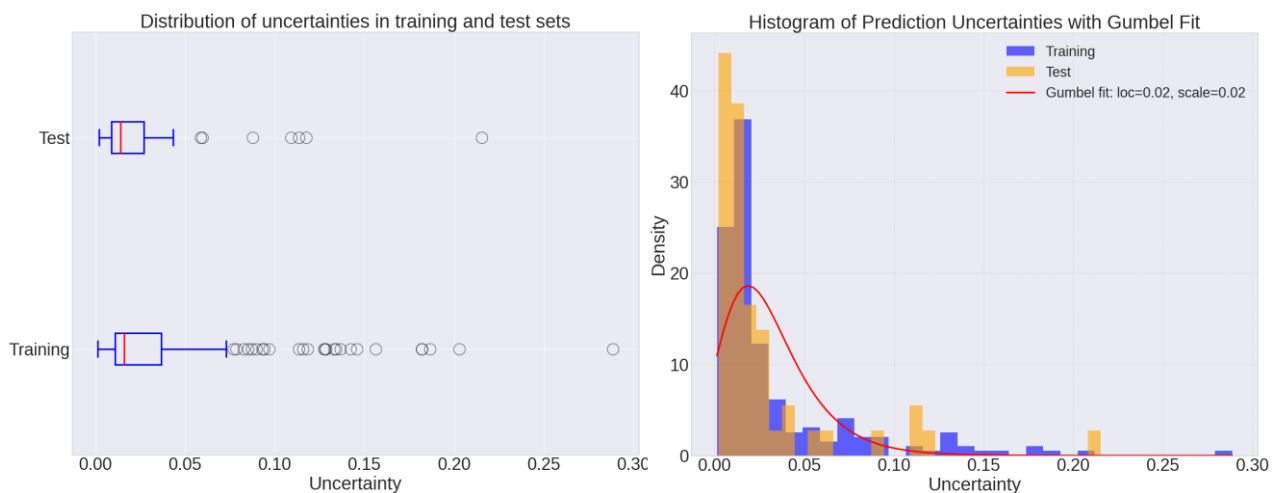


**Figure 15. Distribution of uncertainties: Testing and training | EAAB | Sector III | Belén**

## 12. Results and Discussion

Consequently, Figure 16 illustrates the prediction ability of the BiLSTM model with Monte Carlo Dropout in detecting leaks in the training and test sets. In this graph, the accuracy of the model in the event of leaks is validated. The red crosses represent the actual leak labels in the training set, while the blue circles represent the labels predicted by the model in the same set (left graph). For a correct prediction, these two symbols must match in position, indicating that the model is adequately capturing leaks in the training data. Similarly, on the test set (20%), the orange crosses represent the actual leak labels, and the green circles represent the labels predicted by the model. Matching these symbols in the test set validates the model's ability to generalize and correctly detect leaks in previously unseen data. This graph demonstrates the effectiveness of the BiLSTM-Kalman-Monte Carlo Dropout Model in accurately identifying leaks in urban hydraulic systems, ensuring reliable detection in both training and test data.

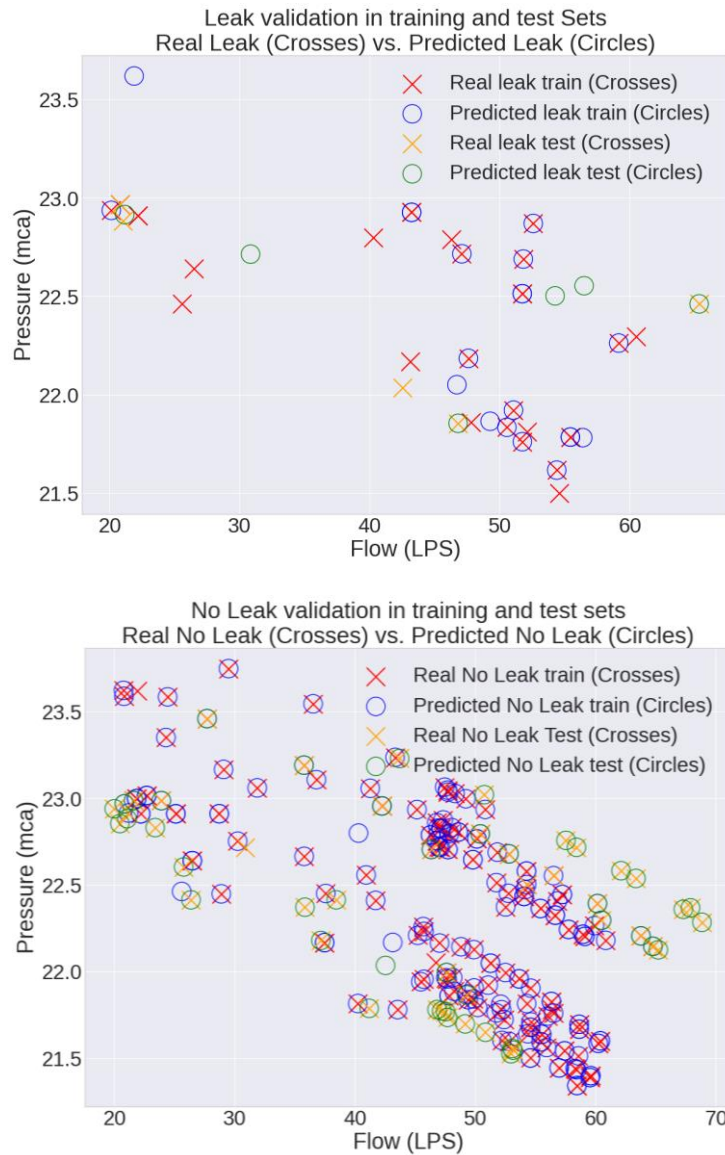


Figure 16. Training and testing: | EAAB | Sector III | Belén

The validation of the model prediction in the absence of leaks in the training and test sets is presented in the right graph. This graph depicts how the BiLSTM model with Monte Carlo Dropout predicts the absence of leaks. The red crosses represent the actual no-leakage labels in the training set, while the blue circles indicate the labels predicted by the model in the same set. For successful prediction, these two symbols must match in location, indicating that the model is adequately capturing the absence of leakage in the training data. Similarly, in the test set (20%), the orange crosses represent the actual no-leakage labels, and the green circles indicate the labels predicted by the model. The match of these symbols in the test set validates the model's ability to generalize and correctly detect the absence of leaks in previously unseen data. This graph demonstrates the effectiveness of the BiLSTM-Kalman-Monte Carlo Dropout model in accurately identifying the absence of leaks in urban hydraulic systems, ensuring reliable detection in both training and test data.

Turkowski et al. (2016) [24] indicated that a system based on uncertainty can evaluate leak detection, minimizing false alarms. The Monte Carlo Dropout model can estimate both the model predictions and the uncertainties associated with the data. This contributes to the interpretability and reliability of the model in machine learning processes. This approach involves performing multiple prediction scenarios on the same input data set while enabling dropout during inference, allowing variability in model predictions to be assessed.

Figure 17 presents the heat map that illustrates the behavior of the uncertainties both during the training phase and in the validation phase of the BiLSTM model with Monte Carlo Dropout for Sector III of the EAAB in Belén. In the heat map corresponding to the training stage (left), it is observed how the uncertainties are distributed as a function of pressure (mca) and flow rate (LPS). The areas with red and yellow colors indicate regions where the model has greater uncertainties in its predictions. For example, Pérez et al. (2016) [25] estimated the uncertainty in the demands to account for the uncertainty observed in the actual measurements. These areas may be affected by noise not detected in the process of filtering the flow and pressure signals.

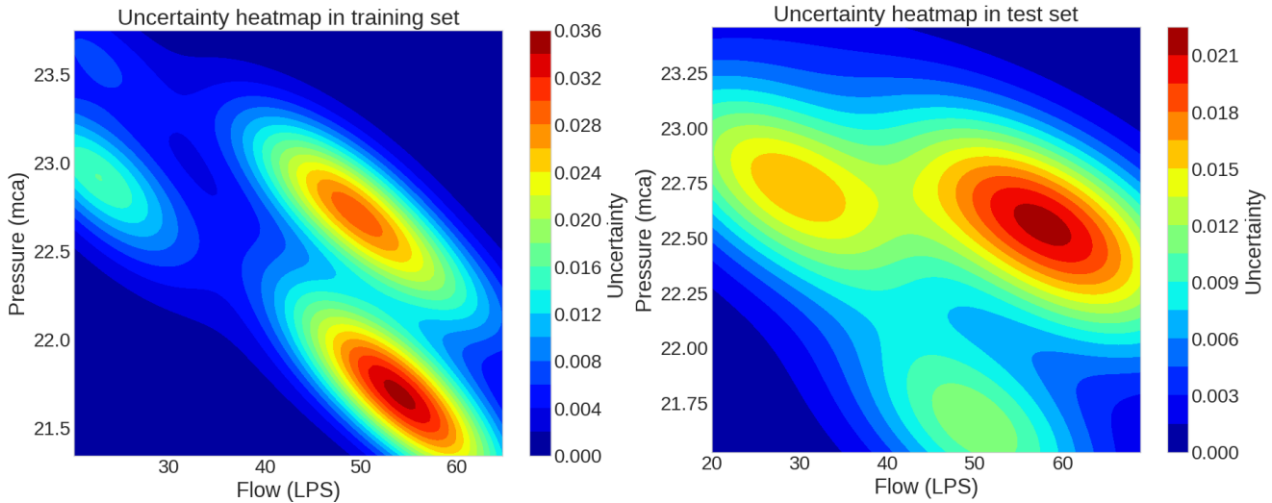


Figure 17. Heat maps | Uncertainty | EAAB | Sector III | Belén

On the other hand, the blue and green areas represent regions of lower uncertainty, suggesting that the model has greater confidence in its predictions in these observed data. Likewise, the heat map of the validation phase (right) follows a similar structure, showing how uncertainties behave when the model is faced with unseen data. Specifically, the behavior of the uncertainties in the interval of  $22.5 < \text{pressure} < 22.75$  mca and  $55 < \text{flow} < 60$  LPS illustrates that the regions with yellow and red colors indicate a relatively high level of uncertainty in the model predictions. This information is crucial to identify areas where the model may need additional improvements or where the data may be influenced by external factors not considered during training.

Figure 18 depicts two heat maps associated with leak detection in the training and validation stages. In the heat map corresponding to the training stage (left), a high density of leak detection is observed in the areas colored in red and orange, indicating that the model has consistently identified leaks in these specific regions of the data space characteristics. These areas are mainly concentrated in the pressure range between 21.8 and 22.8 mca and the flow range between 40 and 60 LPS.

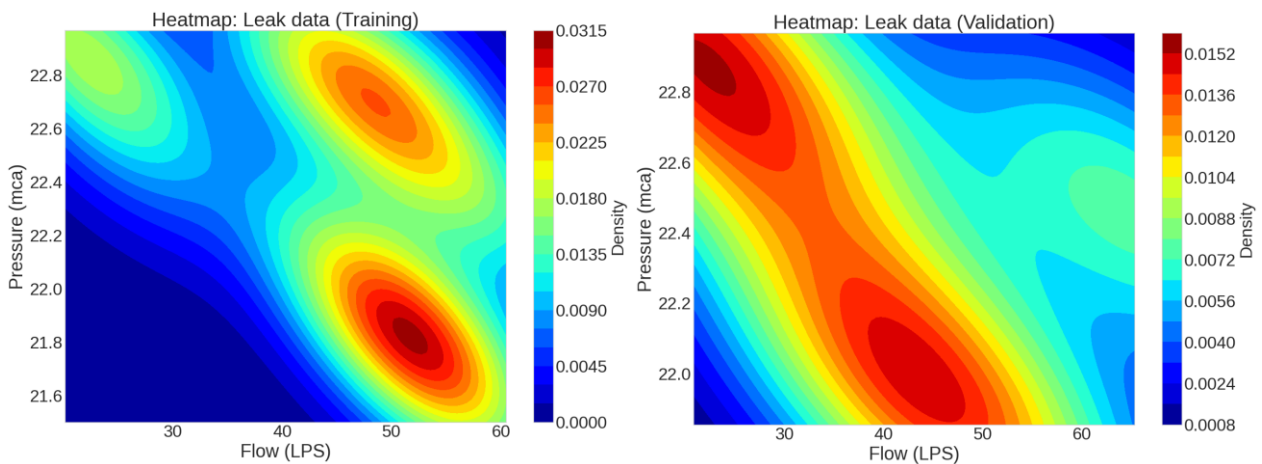


Figure 18. Heat maps | Leaks | EAAB | Sector III | Belén

Similarly, in the heat map corresponding to the validation phase (right), a similar behavior is evident, with the red and orange areas indicating greater leak detection by the BiLSTM model. The consistency between the training and validation stages suggests that the model maintains a robust ability to identify leaks in different data sets, which is crucial to ensure reliability in the practical implementation of the leak monitoring system in urban hydraulic systems.

These areas are mainly found in the pressure range between 22.0 and 22.8 mca and the flow range between 30 and 50 LPS. The similarity in detection patterns between the training and validation maps suggests that the model generalizes well, maintaining its ability to detect leaks in unseen data with high accuracy. The high detection areas in the validation map corroborate the effectiveness of the model in identifying leaks. Finally, Figure 19 presents the maps developed for the absence of leakage for the training and validation data. In the heat map of the training stage (left), the areas in red and orange are highlighted, representing areas with a high data density without leaks. The areas of greatest non-leak detection are mainly concentrated in the pressure range between 21.5 and 23.5 mca and the flow range between 45 and 65 LPS. On the other hand, the validation phase heatmap (right) depicts a similar pattern, with red and orange areas indicating high non-leak detection by the model on unknown data, established in the dataset validation corresponding to 20% of all observed data. These zones are mainly found in the pressure range between 22.0 and 23.25 mca and the flow range between 30 and 55 LPS. The similarity between the training and validation heatmaps suggests that the model maintains its ability to correctly identify leak-free conditions in new observations.

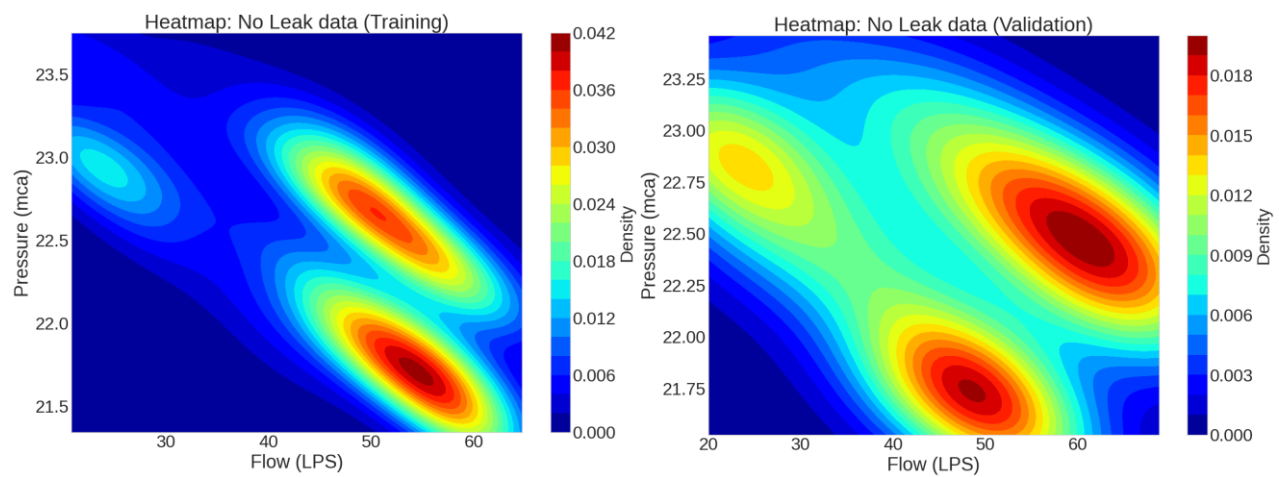


Figure 19. Heat maps | No leaks | EAAB | Sector III | Belén

Table 6 compares various studies on leak detection using artificial neural network (ANN) and BiLSTM techniques. In 2022, Lu et al. [26] present a PPA method based on neural networks for detecting leaks in pipelines, demonstrating considerable accuracy. This approach leverages the ability of neural networks to learn and recognize complex patterns in flow data, which is critical for leak identification. Likewise, Kogbaev et al. [27] and Yang & Zhao (2022) [1]. They apply BiLSTM together with spatiotemporal correlation to detect gas leaks, showing the versatility and efficiency of BiLSTM in different scenarios.

Table 6. Model comparison: BiLSTM and RNA in leak detection

Authors	Study	Model/Technique
Lu et al. (2020) [26]	PPA method for leak detection in pipelines with neural networks	Neural networks
Kopbayev et al. (2022) [27]	Gas leak detection with BiLSTM and spatio-temporal correlation	BiLSTM
Yang & Zhao (2022) [1]	Gas leak detection with BiLSTM and spatio-temporal correlation	BiLSTM
Amora et al. (2022) [28]	Consumption-based water management home with neural networks	Neural networks
Tornyeviadzi et al. (2023) [29]	Analysis of night flow in networks water with supervised learning	Supervised learning
Hao et al. (2023) [30]	Energy data traceability with data analysis and neural networks	Neural networks
Wu et al. (2018) [21]	Detection of leaks in water networks with artificial neural networks	Neural networks
Current Study	Leak detection in urban hydraulic systems using the K-BiLSTM-Monte Carlo Dropout Model	Kalman-BiLSTM-Monte Carlo Dropout

Amora et al. contribute with studies using BiLSTM for pipeline leak detection and discrimination and water consumption management, highlighting the ability of this model to identify leak patterns and optimize water management. These studies highlight the evolution and adaptation of advanced RNA and BiLSTM techniques in the field of leak detection, addressing various applications and contexts. In comparison, this studio an innovative approach by combining BiLSTM with Monte Carlo Dropout and the Kalman filter. This model, called K-BiLSTM-Monte Carlo

Dropout, not only improves the accuracy of leak detection in urban hydraulic systems, but also incorporates uncertainty assessment, representing a significant advance in the field.

The inclusion of the Kalman filter allows for additional signal smoothing and error correction in real time, while the Monte Carlo Dropout offers a robust assessment of uncertainty, improving the adaptability of the model to changing conditions and noisy data. This comprehensive approach allows for more reliable and efficient leak detection, essential for the management and predictive maintenance of hydraulic infrastructures. The study stands out for its ability to handle variability in flow and pressure data, providing an advanced and accurate solution for leak detection. This innovative model marks significant progress over traditional methods, demonstrating the importance of integrating multiple advanced techniques combined with the IoT to address complex challenges in leak detection in water distribution systems.

### 13. Conclusion

The BiLSTM model developed and implemented for leak detection in the hydraulic system illustrates a high capacity for generalization and adequate learning from the data, as evidenced by the significant decrease in training loss and stability in the accuracy and validation loss metrics. Through the detailed analysis of pressure and flow signals, together with the application of techniques such as the Kalman filter and uncertainty evaluation using Monte Carlo Dropout, it has been possible to identify leak patterns with high precision. The integration of these approaches has allowed us to improve the interpretation of trends in time series and reduce the impact of noise on model predictions. The ability of the BiLSTM to analyze data sequences in both directions, combined with the robustness of the Kalman filter for signal stabilization and uncertainty evaluation, ensures that the model not only predicts with high accuracy but also provides a measure of confidence in their predictions.

Wavelet spectrogram analysis of the flow signal reveals significant information about the energy behavior of the hydraulic system and leak detection. The drastic reduction in system energy towards the end of time is related to energetic alterations in terms of pressure and flow. The spectrogram illustrates an energetic decay in the low frequencies of the signal, suggesting the presence of a disturbing event, such as a leak. Similarly, for pressure, the wavelet spectrogram depicts the energy front produced by pressure disturbances, evidencing behavior similar to that observed in the flow signal. Fluctuations in the energy of the pressure signal indicate the presence of leak events, where a significant increase in energy is observed followed by a stabilization. This spectral analysis is essential to identify and characterize leaks, as it allows us to observe how leaks occur. Disturbances affect the energy of signals at different frequencies and times. The ability of the wavelet spectrogram to decompose the signal into time-frequency components facilitates early and accurate leak detection, providing a powerful tool for monitoring and predictive maintenance of urban hydraulic systems.

The K-BiLSTM-MC model implemented in Hydraulic District III - EAAB, specifically in Sector III Belén, has demonstrated a high capacity to detect anomalies in pressure and flow signals. Using the Isolation Forest algorithm, anomalous data points were identified that indicated possible leaks in the system. These anomalies occurred in specific patterns, evidencing the effectiveness of the model in monitoring and reacting to sudden changes in the operating conditions of the hydraulic system. The model architecture, which includes layers of recurrent neural networks (LSTM) and the use of Monte Carlo Dropout for uncertainty evaluation, has shown strong performance with low loss in both training and validation. The predictive model demonstrates a high capacity for generalization and adaptation to unknown data.

### 14. Declarations

#### 14.1. Author Contributions

Conceptualization, C.A.G.U. and E.O.L.M.; methodology, C.A.G.U., E.O.L.M., and E.O.L.M.; software, E.O.L.M.; validation, E.O.L.M.; formal analysis, C.A.G.U., E.O.L.M., and E.O.L.M.; investigation, E.O.L.M.; data curation, C.A.G.U. and E.O.L.M.; writing—original draft preparation, C.A.G.U., E.O.L.M., and E.O.L.M.; writing—review and editing, C.A.G.U., E.O.L.M., and E.O.L.M.; visualization, E.O.L.M.; supervision, E.O.L.M. All authors have read and agreed to the published version of the manuscript.

#### 14.2. Data Availability Statement

Data supporting the findings of this study are available upon request from the corresponding authors.

#### 14.3. Funding

The authors received no financial support for the research, authorship, and/or publication of this article.

#### 14.4. Acknowledgements

The authors express their gratitude to the Head of the Aqueduct Service Division Zone 3 of the Bogotá Aqueduct and Sewer Company (EAAB- Bogotá, Colombia), for their support in this study and for providing access to information on pressures and flows in the hydraulic sector.

## 14.5. Conflicts of Interest

The authors declare no conflict of interest.

## 15. References

- [1] Yang, L., & Zhao, Q. (2022). A BiLSTM Based Pipeline Leak Detection and Disturbance Assisted Localization Method. *IEEE Sensors Journal*, 22(1), 611–620. doi:10.1109/jsen.2021.3128816.
- [2] Zhang, X., Shi, J., Yang, M., Huang, X., Usmani, A. S., Chen, G., Fu, J., Huang, J., & Li, J. (2023). Real-time pipeline leak detection and localization using an attention-based LSTM approach. *Process Safety and Environmental Protection*, 174, 460–472. doi:10.1016/j.psep.2023.04.020.
- [3] Yang, L., & Zhao, Q. (2020). A Novel PPA Method for Fluid Pipeline Leak Detection Based on OPELM and Bidirectional LSTM. *IEEE Access*, 8, 107185–107199. doi:10.1109/ACCESS.2020.3000960.
- [4] Wang, L., Hu, C., Ma, T., Yang, Z., Guo, W., Mao, Z., Guo, J., & Li, H. (2024). GTFE-Net-BiLSTM-AM: An intelligent feature recognition method for natural gas pipelines. *Gas Science and Engineering*, 125. doi:10.1016/j.gjsce.2024.205311.
- [5] Gao, Y., Piltan, F., & Kim, J.-M. (2022). A Hybrid Leak Localization Approach Using Acoustic Emission for Industrial Pipelines. *Sensors*, 22(10), 3963. doi:10.3390/s22103963.
- [6] Guo, X. L., Yang, K. L., & Guo, Y. X. (2012). Leak detection in pipelines by exclusively frequency domain method. *Science China Technological Sciences*, 55(3), 743–752. doi:10.1007/s11431-011-4707-3.
- [7] Ullah, N., Ahmed, Z., & Kim, J.-M. (2023). Pipeline Leakage Detection Using Acoustic Emission and Machine Learning Algorithms. *Sensors*, 23(6), 3226. doi:10.3390/s23063226.
- [8] Shen, Y., & Cheng, W. (2022). A Tree-Based Machine Learning Method for Pipeline Leakage Detection. *Water*, 14(18), 2833. doi:10.3390/w14182833.
- [9] Acharya, T., Annamalai, A., & Chouikha, M. F. (2023). Efficacy of Bidirectional LSTM Model for Network-Based Anomaly Detection. 2023 IEEE 13<sup>th</sup> Symposium on Computer Applications & Industrial Electronics (ISCAIE), Penang, Malaysia. doi:10.1109/iscaie57739.2023.10165336.
- [10] Lee, S., & Kim, B. (2023). Machine Learning Model for Leak Detection Using Water Pipeline Vibration Sensor. *Sensors (Basel, Switzerland)*, 23(21), 8935. doi:10.3390/s23218935.
- [11] Chumchu, P. (2021). A Leak Detection in Water Pipelines Using Discrete Wavelet Decomposition and Artificial Neural Network. *Advances in Signal Processing and Intelligent Recognition Systems*, 49–65. doi:10.1007/978-981-16-0425-6\_4.
- [12] Barandouzi, M. A., Mahinthakumar, G., Ranjithan, R., & Brill, E. D. (2012). Probabilistic Mapping of Water Leakage Characterizations Using a Bayesian Approach. *World Environmental and Water Resources Congress 2012*. doi:10.1061/9780784412312.326.
- [13] Proença, M., Paschoalini, A. T., & Obata, D. H. S. (2023). Prediction of the probabilistic water leak location in underground pipelines using Monte Carlo simulation. *Water Practice and Technology*, 18(3), 522–535. doi:10.2166/wpt.2023.026.
- [14] Zhang, Z., & Lv, M. (2022). Leakage prediction of water supply network based on SAA-SVM model. *Journal of Physics: Conference Series*, 2202(1), 012014. doi:10.1088/1742-6596/2202/1/012014.
- [15] Zhang, P., He, J., Huang, W., Zhang, J., Yuan, Y., Chen, B., Yang, Z., Xiao, Y., Yuan, Y., Wu, C., Cui, H., & Zhang, L. (2023). Water Pipeline Leak Detection Based on a Pseudo-Siamese Convolutional Neural Network: Integrating Handcrafted Features and Deep Representations. *Water*, 15(6), 1088. doi:10.3390/w15061088.
- [16] Abdul, Z. K., & Al-Talabani, A. K. (2022). Mel frequency cepstral coefficient and its applications: A review. *IEEE Access*, 10, 122136–122158. doi:10.1109/ACCESS.2022.3223444.
- [17] Koolagudi, S. G., Rastogi, D., & Rao, K. S. (2012). Identification of language using mel-frequency cepstral coefficients (MFCC). *Procedia Engineering*, 38, 3391–3398. doi:10.1016/j.proeng.2012.06.392.
- [18] Koutsyiannis, D. (2012). A Monte Carlo approach to water management. *Proceedings of the Geophysical Research Abstracts, European Geosciences Union General Assembly, 22-27 April, 2012, Vienna, Austria*.
- [19] Thu, S., Aung, N., & Ko, K. (2023). A Calibration Technique for Water Flow Sensor YF-S201 1. *International Journal of Trend in Research and Development*, 5(5), 152–154.
- [20] Zahran, A., Hassan Rabie Sakr, L., Shabaka, I., & Mansour, M. (2020). Performance of an Orifice Meter Handling Two-Phase (Gas-Liquid) Flow. (Dept. M). *Mansoura Engineering Journal*, 45(3), 29–38. doi:10.21608/bfemu.2020.114002.

- [21] Wu, Y., Liu, S., Smith, K., & Wang, X. (2018). Using Correlation between Data from Multiple Monitoring Sensors to Detect Bursts in Water Distribution Systems. *Journal of Water Resources Planning and Management*, 144(2), 04017084. doi:10.1061/(asce)wr.1943-5452.0000870.
- [22] Shao, Y., Li, X., Zhang, T., Chu, S., & Liu, X. (2019). Time-series-based leakage detection using multiple pressure sensors in water distribution systems. *Sensors (Switzerland)*, 19(14), 3070. doi:10.3390/s19143070.
- [23] Sun, Q., Zhang, Y., Lu, B., & Liu, H. (2022). Flow Measurement-Based Self-Adaptive Line Segment Clustering Model for Leakage Detection in Water Distribution Networks. *IEEE Transactions on Instrumentation and Measurement*, 71, 1–13. doi:10.1109/TIM.2022.3165258.
- [24] Turkowski, M., Bratek, A., & Ostapkowicz, P. (2016). Uncertainty Analysis as the Tool to Assess the Quality of Leak Detection and Localization Systems. *Recent Global Research and Education: Technological Challenges*, 469–475, Springer, Cham, Switzerland. doi:10.1007/978-3-319-46490-9\_62.
- [25] Perez, R., Cuguero, J., Blesa, J., Cuguero, M. A., & Sanz, G. (2016). Uncertainty effect on leak localisation in a DMA. 2016 3<sup>rd</sup> Conference on Control and Fault-Tolerant Systems (SysTol), Barcelona, Spain. doi:10.1109/systol.2016.7739770.
- [26] Lu, H., Iseley, T., Behbahani, S., & Fu, L. (2020). Leakage detection techniques for oil and gas pipelines: State-of-the-art. *Tunnelling and Underground Space Technology*, 98, 103249. doi:10.1016/j.tust.2019.103249.
- [27] Kopbayev, A., Khan, F., Yang, M., & Halim, S. Z. (2022). Gas leakage detection using spatial and temporal neural network model. *Process Safety and Environmental Protection*, 160, 968–975. doi:10.1016/j.psep.2022.03.002.
- [28] Amora, D. J. A., Janapin, M. A. V., Calayag, B. A. M., Rioflorido, C. L. P. P., Estur, N. M., & Villegas, P. A. L. (2022). Design of a Household Consumption based Water Leak Detection System Utilizing Machine Learning Algorithm. 2022 IET International Conference on Engineering Technologies and Applications (IET-ICETA), Changhua, Taiwan. doi:10.1109/iet-iceta56553.2022.9971564.
- [29] Tornyeviadzi, H. M., Mohammed, H., & Seidu, R. (2023). Robust night flow analysis in water distribution networks: A BiLSTM deep autoencoder approach. *Advanced Engineering Informatics*, 58, 102135. doi:10.1016/j.aei.2023.102135.
- [30] Hao, J., Jin, M., Li, Y., Piao, T., Hu, H., Xi, X., & Chen, J. (2023). Power Data Traceability Mechanism Based on Data Processing Unit. 2023 IEEE 11th Joint International Information Technology and Artificial Intelligence Conference (ITAIC), Chongqing, China. doi:10.1109/itaic58329.2023.10408832.

## Appendix I: Python Encoding ®: Model K-BiLSTM-MC

Francisco José de Caldas District University (Bogotá, Colombia)  
 Faculty of Technology | Civil Engineering  
 Edgar O. Ladino M. | eoladinom@udistrital.edu.co  
 www.edgarladino.com  
 Model K-BiLSTM-MC

```
-----//

----- Leak detection in urban hydraulic systems using the K-BiLSTM-Monte Carlo Dropout Model
-----//

archivo_csv = '/content/drive/MyDrive/Modelo-EAAB/RNA-Belen/Serie_Presion_Caudal_Belen_etiquetados-5.csv'
datos = pd.read_csv(archivo_csv, encoding='ISO-8859-1')
datos_pca = datos[['Tiempo (horas)', 'Presión (mca)', 'Caudal (LPS)', 'Etiqueta Fuga (Fuga= 1; Sin Fuga= 0)']]
datos_pca['Presión (mca)'] = apply_kalman_filter(datos_pca['Presión (mca)'].values)
datos_pca['Caudal (LPS)'] = apply_kalman_filter(datos_pca['Caudal (LPS)'].values)
def apply_kalman_filter(data):
    kf = KalmanFilter(initial_state_mean=0, n_dim_obs=1)
    state_means, _ = kf.filter(data)
    return state_means.flatten()
scaler = MinMaxScaler()
features_scaled = scaler.fit_transform(datos_pca[['Tiempo (horas)', 'Presión (mca)', 'Caudal (LPS)']])
labels = datos_pca['Etiqueta Fuga (Fuga= 1; Sin Fuga= 0)'].values
def create_sequences(features, labels, window_size=10):
    X, y = [], []
    for i in range(len(features) - window_size + 1):
        X.append(features[i:(i + window_size)])
        y.append(labels[i + window_size - 1])
    return np.array(X), np.array(y)
window_size = 10
X, y = create_sequences(features_scaled, labels, window_size)
X_train, X_test, y_train, y_test = train_test_split(X, y, test_size=0.2, random_state=42)
model = Sequential([
    Bidirectional(LSTM(50, return_sequences=True), input_shape=(window_size, 3)),
    Dropout(0.5),
    Bidirectional(LSTM(50)),
    Dropout(0.5),
    Dense(1, activation='sigmoid')
])
model.compile(optimizer='adam', loss=MeanSquaredError(), metrics=['accuracy', MeanAbsoluteError()])

history = model.fit(X_train, y_train, epochs=200, batch_size=64, validation_split=0.2)

def predict_with_uncertainty(model, X, n_iter=100):
    result = np.zeros((n_iter,) + (X.shape[0], 1))
    for i in range(n_iter):
        result[i] = model(X, training=True)
    prediction = result.mean(axis=0)
    uncertainty = result
```